University of South-Eastern Norway

www.usn.no

FMH606 Master's Thesis 2023

Energy and Environmental Technology

Ammonia vent handling for carbon-free shipping

Whitney Ndidi Ezeani Ezeani

Faculty of Technology, Natural sciences and Maritime Sciences

Campus Porsgrunn

University of South-Eastern Norway

www.usn.no

Course: FMH606 Master's Thesis, 2023

Title: Ammonia vent handling for carbon-free shipping

Number of pages: 47

Keywords: Ammonia, hydrogen, combustion, laminar flame speed.

Student: Whitney Ndidi Ezeani Ezeani

Supervisor: Joachim Lundberg

External partner: Wärtsilä Moss AS

Summary:

The challenges of reducing greenhouse gas emissions in the growing maritime industry are substantial to reach the Paris Agreement and keep the global temperature rise below 2 ^{o}C. Alternative fuels, such as hydrogen, are considered to substitute traditional hydrocarbon fuels since their combustion produces water. However, hydrogen storage and delivery are complicated and ammonia is considered a critical component to accelerate the transition. Due to the high toxicity of ammonia, stronger regulations are in place and some emissions limits range from 30 or 25 ppm depending on different factors and exposure time. This project intents to study the combustion process of ammonia for a two-step combustion unit aimed to be installed in vessels.

Experiments with two different combustion unit geometry are conducted and simulations with Cantera are executed by using Konnov, Gri-Mech 3.0 mechanism for ammonia and the h2o2 mechanism for hydrogen.

The results reveal that operating in close to adiabatic conditions higher temperatures, greater hydrogen compositions, fastest burning velocities and lower heat loss are achieved. Nitrous oxide composition increases by the injection of extra nitrogen but decreases while operating in slightly rich-fuel combustions. In lean-fuel combustions, smaller quantities of hydrogen are also observed.

Finally, the ammonia content in the exhaust gas is less than 30 ppm for rich and lean combustions.

Preface

This report is the documentation of the Master's Thesis conducted at the University of South-Eastern Norway, Porsgrunn during the spring of 2023. The Thesis is a partial requirement to obtain the master's degree in Energy and Environmental Technology, it is partnered with Wärtsilä Moss AS and collects details of experiments and simulations of an ammonia combustion unit.

First and foremost, I would like to praise and thank God, the Almighty, who has granted countless blessings, knowledge and opportunities to the writer.

I would like to extend my sincere appreciation to my supervisor Joachim Lundberg, whose guidance, patience, comprehension and expertise have been invaluable throughout this journey. His constant support, encouragement and insightful feedback have been instrumental in the success of this report. I am truly grateful for his mentorship and the trust he placed in me for the fulfilment of this research.

I am extremely grateful to both the University and Wärtsilä Moss AS for granting me the opportunity to work on this report. I would like to express my gratitude to the faculty members whose knowledge and expertise have shaped my academic growth, to Odd Ivar Lindløv and to the participants who willingly dedicated their time and shared their valuable insights.

Finally, I would like to express my gratitude to my family and friends, for their assistance and encouragement. Their belief in my abilities and unwavering support have provided me with the strength to overcome challenges and persevere. I am truly blessed to have such amazing humans in my life.

Porgrunn, 14/05/2023

Whitney Ndidi Ezeani Ezeani

List of figures

List of tables

Contents

1 Introduction

Scientists have agreed for decades on the challenges and necessity of decarbonizing the current global energy system to minimize greenhouse gas (GHG) emissions. The shipping sector continues to be a substantial source of GHG accounting for 2-3% of the total emissions. It is predicted that the sector will grow in parallel with the expansion of global commercialization trade, making it difficult to meet the Paris Agreement's goal of keeping global warming well below 2ºC, and ideally to 1.5ºC. The idea is to replace the actual consumption rate of fossil fuels, therefore promoting a carbon-free fuel system for the maritime industry.

Hydrogen (H_2) is the element which can better substitute the actual hydrocarbon fuels due to its zero carbon emission. However, H_2 storage and transportation are complex and additional complexity is found by the requirement of vast amounts of power to manufacture it, either in its gaseous or liquid form, constricting its economic feasibility as a fuel. For its part, lithium battery storage has insufficient capacity to cope with the rising demand. Chemical hydrogen storage via its derivatives, on the other hand, will be crucial in decarbonizing the transportation industry. Ammonia (NH_3) is regarded as a key hydrogen storage component. It offers around 17.7% weight of hydrogen content and greater hydrogen density per volume than liquid hydrogen. However, some of the downsides of ammonia include its low burning laminar velocity and the generation of nitrous oxides. Understanding its combustion mechanism is critical to ensuring optimal efficiency and circumstances to satisfy its regulatory requirement.

1.1 Background

While numerous projects are investigating battery technology for short-haul transportation, hydrogen is most likely to be the only viable carbon-free fuel for long-haul shipping. [1][2] However, due to its low energy density hydrogen is a less lucrative fuel for the maritime industry since carrying enough fuel displaces an excessive amount of cargo.

Various techniques of storing hydrogen compounds are explored to attain a carbon-neutral future. To facilitate storage and transportation, hydrogen can be incorporated into a carrier. [3] Chemical hydrogen storage can be accomplished by molecules containing considerable quantities of hydrogen, also known as liquid hydrogen carriers, which are liquid at temperatures and pressures near the ambient. Both liquid natural gas (LNG) and liquid NH_3 have high density of hydrogen storage and are continuously transported throughout the worldwide via trucks or ships. [4] Although only the former is carbon-free and contains 108 kg H_2/m^3 at 293 K and 8.6 bars, its combustion has the major disadvantage of producing nitrous oxides (NO_x), which is an important greenhouse gas. [5] Furthermore, ammonia has additional requirements due to its toxicity compared to methane. According to the USA Environmental Protection Agency (EPA), its Acute Exposure Guideline Level 1 (AEGL1) has established a hazardous limit of 30 ppm. [6] Permissible Exposure Limits (PEL) are set to be 50 ppm and Recommended Exposure Limits (REL) at 25 ppm, both vary by exposure time. 300 ppm represents the limit for Immediate Danger to Life or Health (IDLH).

1.2 Problem statement

The ammonia storage system will require significantly more storage volume than other fuels because of its properties. Due to its high toxicity and the evaporation of the gas during its storage, the tank must also be supplemented with vent lines and therefore, a treatment system to release the element as the pressure in the tanks rises. Adopting the appropriate procedures

will prevent emissions from exceeding regulatory limits and an excessive increase in the weight of the maritime vehicle. Because NH_3 has a very strong policy of release to the atmosphere in small concentrations in comparison to fossil fuels of 30 ppm, it is necessary to develop the appropriate equipment to ensure vessel safety and mitigation of adverse effects in the environment without compromising ship efficiency transport.

1.3 Objective

The main goal of this project is to investigate the thermal decomposition of ammonia and therefore the operation of a pilot combustor, to assess the feasibility of implementing the equipment at the end of an ammonia vent treatment line in a vessel. The research focuses on analyzing a premix ammonia/air mixture and its product emissions, such as NO_x, in certain circumstances.

1.4 Scope

The scope of the report is to determine how the Wärtsilä pilot combustion reactor system degrades surplus NH_3 purged from a storage buffer tank into mostly nitrogen and water to discharge it below the legal limit, being the target below 30 ppm. The process will be focused on the rich fuel combustion of the NH_3 and/or $NH_3 - N_2$ mixture since the storage is ammonia and includes no hydrocarbons. The study is further supported by simplified 1D flame simulations in Cantera version 2.6.0 and experiments in the pilot scale reactor.

1.5 Research outline

The thesis is organized into 6 chapters and appendices.

Chapter 1 is the introduction and general information about the project.

Chapter 2 includes a review of the literature and some previous works, the basic theory related to the thermal decomposition of ammonia including thermodynamics and kinetic mechanisms and the usefulness of ammonia in decarbonizing the marine sector.

Chapter 3 is the explanation and methodology followed to carry out the experiments.

Chapter 4 gathers information about the conditions and simulation procedure.

Chapter 5 shows all the results achieved, explanations, sensitivity analysis and discussion of this project.

The final, Chapter 6, is the conclusion of the project.

2 Literature review

The energy transitions and the need to abate greenhouse gas emissions drive further research into ammonia as a source of hydrogen and therefore as a fuel. Today, it is one of the most widely manufactured chemicals, with over 70% destined for agricultural usage as a fertilizer, while the remainder is employed in various industrial applications such as explosives, cleaning goods, synthetic fibres, etc. [7] As shown in Figure 2.1, the ammonia consumption in the energy market is expected to increase exponentially as hydrogen demand increases. [3] Around 33Mt/yr of hydrogen is used annually to produce NH_3. However, the adverse factors of using ammonia are the nitrogen oxides emissions, mostly as nitric oxide (NO), nitrogen dioxide (NO_2) and nitrous oxide (N_2O), formed from the combustion processes. [8].

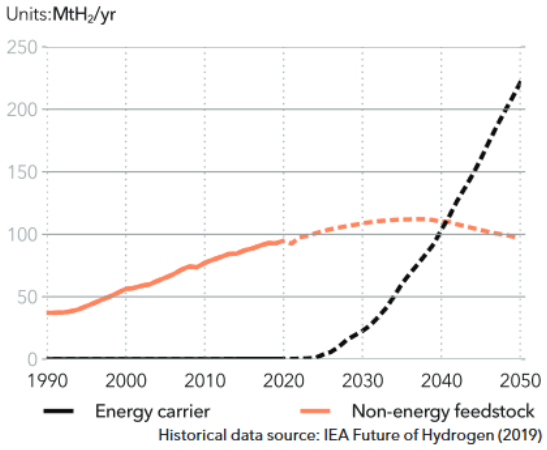

Figure 2.1: Global demand for hydrogen and its derivatives by purpose. [3]

P. Glarborg, James A. Miller and colleagues [8] established and assessed, based on the work of nitrogen chemistry, a non-optimized chemical kinetic model for the homogenous nitrogen chemistry in combustion. Different models were used to analyze key reaction stages and the predictive capability of the mechanism. The models were then validated with a set of experimental data. The experimental settings were precise enough to allow a kinetic interpretation. Their research also focused on the combined chemistry of nitrogen and light hydrocarbons such as methane (CH_4) at atmospheric or sub-atmospheric pressures.

Due to the low burning velocity of ammonia and complications with ammonia combustion, Chai et al. [5] investigated the effects of adding hydrogen and methane to enhance the combustion process. They mainly assessed the resulting burning velocity compared to the ammonia-air system, the impacts and limitations of each system and the comparison between both systems. They established the theoretical path reference for transitioning into practical applications.

Valera-Medina et al. [9] highlight previous relevant studies of combustion and challenges of ammonia for power application and different technologies, such as CO_2 removal, working fluid for power cycles fuel cells, gas turbines and propulsion technology. It covers from the initial attempts of ammonia for power to safety aspects, corrosiveness, ammonia mixture with carbon based fuels, etc. On the other hand, another previous research Valera-Medina et al. [10] presents the results of the computational and experimental behavior of the flame of a 50:50 $NH_3 - H_2$ premixed lean mixture where high levels of NO_x. [10][10]

2.1 Properties of ammonia

Anhydrous ammonia, commonly known as ammonia, is a colorless, hygroscopic substance with a strong odor and is highly toxic. Because of its alkaline properties, it is exceedingly corrosive and cautious material selection is required to handle it. It corrodes galvanized metals, copper and copper alloys, brass and cast iron. [11] [12]

It has a boiling point of -33 ºC, indicating that it is a gas at room temperature. It is flammable but difficult to ignite. [11] It can be transported in its liquid state either in refrigerated storage at atmospheric pressure or compressed containers.

Concerning the safety aspect to handle ammonia as a fuel, its properties are shown in Table 2.1, where it is also compared to other fuels such as methane and hydrogen.

Table 2.1: Ammonia, methane and hydrogen properties in the gaseous phase. [11] [12] [13] [14]

Properties	Units	Ammonia	Methane	Hydrogen
Formula		NH_3	CH_4	H_2
Molecular weight	g/mol	17.03	16	2.02
Boiling temperature (@ 1 bar)	℃	-33	-162	-253
Density (@ boiling temp.)	t/m^3	0.68	0.43	-
Lower heating value	MJ/kg	18.6	50	120.1
Autoignition temperature	℃	651	537	520
Flash point	℃	-33.4	-184.4	N/A
Flammability range	%	15-28	5.3-17	1.0-71
Octane	-	110	107	>130
Minimum ignition energy	MJ	8	0.27	0.018
Solubility in water (@ 20ºC)	g/l	531	0	0
Laminar burning velocity(S_L)	m/s	0.07	0.37	2.91
Main hazards		Toxic	Explosive	Flammable
		Explosive	Cryogenic	Explosive
		Corrosive	Flammable	Buoyancy
		Flammable	Asphyxiating	Propensity to leak

Figure 2.2 illustrates different laminar velocities of ammonia/air premix mixtures determined for various equivalence ratios acquired from various studies. Whilst Roney, Pfahl, Hayakawa, Davis, Takizawa, Mei, Lhuillier, and Ji conducted their tests in a constant volume combustion chamber, Han conducted the measurement by using the heat flux method. The majority of the researches achieve the greatest values of the laminar burning velocity at an equivalency ratio of about 1.1. [15]

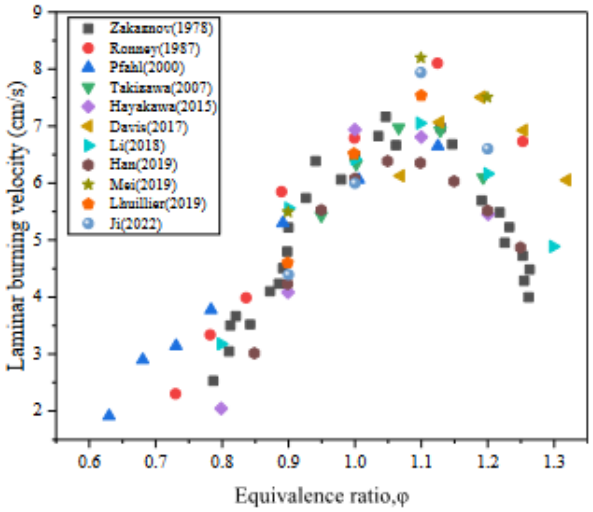

Figure 2.2: Measured laminar burning velocity of NH_3/air mixture at a temperature of 303 K and 1 atm. [15]

2.2 Treatment processes of ammonia

Ammonia gas is released from a variety of industrial sources, including wastewater treatment facilities, chemicals, transportation, agriculture and farming. The Globally Harmonized System of Classification and Labeling of Chemicals (GHS) classifies it as hazardous to aquatic life and with long-term impacts. [11] As a result, the handling of discharging ammonia vapor into water or the atmosphere is done by different techniques depending on the concentration to meet the legislative requirements. They are mainly grouped in absorption techniques such as scrubbers, adsorption treatment as activated carbon, membrane separation techniques, oxidation and catalytic systems with non-noble metals for example Ni as an alternative to Ru-catalysis to decompose into H_2.[16] [4] [17] [18] The scrubber, which is represented in Figure 2.3 in a typical arrangement, treats the gas with an aqueous acid solution. [19] [20]

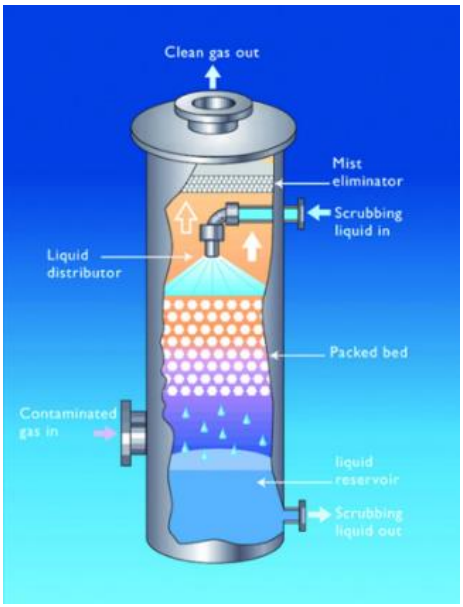

Figure 2.3: Schematic view of a packed bed scrubber [20]

In the last two decades, the rise of LNG fuel ships has also fueled the development of gas combustion units (GCUs) for managing LNG boil-off gas. [21]. GCUs are specifically

designed for releasing surplus gas into the atmosphere through controlled combustion. [22] They may be created compactly, saving important ship surface area. [23]

Figure 2.4 depicts the graphical representation of the main components of a gas combustion unit, where a burner operates in a wide-range flow of surplus gas and nitrogen content when needed. [24] Air fans provide air for combustion and exhaust gas cooling. A gas supply system to manage the gas flow, which can also be combined with the air mass flow; and a combustion chamber to contain the flame.

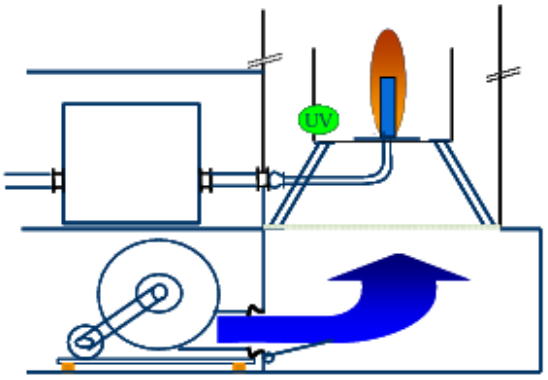

Figure 2.4: Main components of a gas combustion unit. [24]

2.3 Combustion

The process by which a fuel is partially or completely oxidized with air is known as combustion. [25] The combustion process can take place under rich fuel conditions, which have a smaller proportion of air relative to the fuel, or under lean fuel conditions, which have a greater air concentration. Stoichiometric combustion occurs when the proportions of air and fuel are theoretically identical, as in the stoichiometric reaction. The amount of fuel in a mixture is determined by Equation (2.1) the fuel-air ratio parameter (f)

$$f = \frac{m_f}{m_a} \tag{2.1}$$

where m_f and m_a are the respective masses of the fuel and air.

The equivalency ratio (ϕ), denoted by Equation (2.2), is the parameter that indicates whether the combustion is lean, stoichiometric, or rich. It is the normalization of the actual fuel-air ratio (f) and the stoichiometric fuel-air ratio (f_s) denoted by Equation (2.3).

$$\phi = \frac{f}{f_s} \tag{2.2}$$

$$f_s = \frac{m_f}{m_a}\Big|_s \tag{2.3}$$

2.3.1 Mass conservation equation

Considering that there is no accumulation in the control volume, the mass conservation equation in the GCU may be represented by Equation (2.4).

$$m_f + m_a = m_p \tag{2.4}$$

where m_f, m_a and m_p are the respective masses of the fuel, air and products.

The species conservation Equation (2.5) is used to calculate the composition of the products, where the limiting reactant controls how much of each component is generated.

$$n_{in} + n_g = n_p \tag{2.5}$$

where n_{in}, n_g and n_p are the respective inflow, generated and product moles.

2.3.2 Mixture composition properties

The thermodynamic properties of a mixture of gases are described through the properties of the corresponding pure substance present in the mixture and can be calculated as shown in Equations (2.6)- (2.9).

$$m = \sum_{i=1}^{K} m_i \tag{2.6}$$

where: m is total mass and m_i is the mass of the species i.

The relative mass amount of a given species i in terms of mass fraction (y_i), is described by Equation (2.7)

$$y_i \equiv \frac{m_i}{m} \tag{2.7}$$

The number of moles of a given species (N_i) can be calculated by Equation (2.8)

$$N_i = \frac{m_i}{Mw_i} \tag{2.8}$$

where Mw_i is the molecular weight of the species i.

At the same time, the total number of moles in a mixture (N) is computed by the expression in Equation (2.9), where N_i is the number of moles of the species i.

$$N = \sum_{i=1}^{K} N_i \tag{2.9}$$

The relative amount of a given species is described in Equation (2.10) by the mole fraction x_i.

$$x_i \equiv \frac{m_i}{m} \tag{2.10}$$

Finally, due to the high temperatures and low pressures, the gas mixture follows the ideal gas law as shown in Equation (2.11).

$$PV = NRT \tag{2.11}$$

Where P is pressure, V volume of the mixture N is the total amount of moles in the mixture, R is the gas constant with the value of 8.134 J/(mol·K) and T is the temperature in kelvin.

2.3.3 Kinetic analysis

Various studies on ammonia combustion have been conducted during the last few decades. Beginning in the 1980s, researchers attempted to understand the pyrolysis of ammonia. Miller et al, as well as other scientists, laid the groundwork for the ammonia combustion and oxidation mechanism as it is depicted in Figure 2.5. [5]

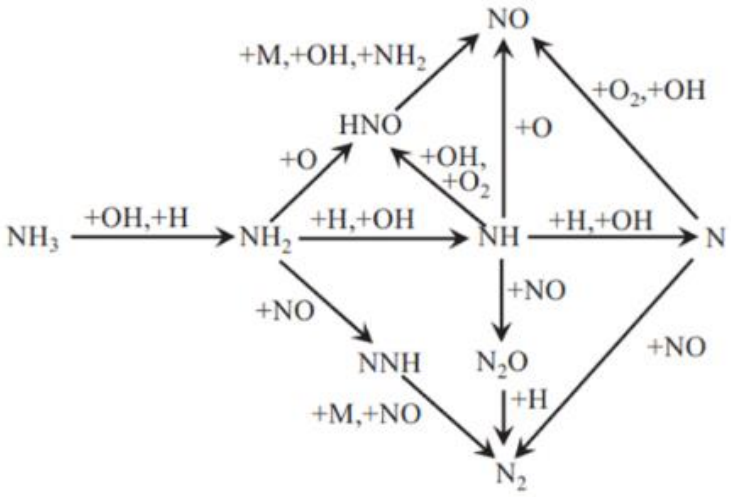

Figure 2.5: Miller mechanism diagram. [5]

When burning ammonia, the ideal chemical reaction route is total oxidation, which generates steam, nitrogen and heat [26] as described in reaction R-2.1. [12]

$$NH_{3(g)} + \frac{3}{4}(O_2 + 3.76N_2) \rightarrow \frac{3}{2}H_2O + 3.32N_2 \qquad \text{R-2.1}$$

However, due to the complications related to burning ammonia and depending on whether the combustion is done in rich or lean circumstances, products such as NO_x, N_2O, H_2 or even NH_3 might be inevitably produced in the actual composition. [5] Thus, the partial oxidation of ammonia favorable under lean conditions normally follows the reaction R-2.2. [26]

$$2NH_{3(g)} + 2.5(O_2 + 3.76N_2) \rightarrow 2NO + 3H_2O + 9.4N_2 \qquad \text{R-2.2}$$

The main concern in lean combustion is the production of NO, where the Zeldovich mechanism, also known as thermal NO, is the major source of NO in high-temperature gas combustion. [8] As seen in reaction R-2.3, it begins with an oxygen atom attacking the triple bond in N_2. The nitrogen is then oxidized to NO by reacting with OH or O_2 as indicated in reactions R-2.4 and R-2.5. Table 2.2 shows the kinetic parameters for the Zeldovich mechanism.

$$O + N_2 \leftrightarrow NO + N \qquad \text{R-2.3}$$

$$N + OH \leftrightarrow NO + H \qquad \text{R-2.4}$$

$$N + O_2 \leftrightarrow NO + O \qquad \text{R-2.5}$$

Table 2.2: Kinetic parameters for the Zeldovich mechanism in the modified Arrhenius expression $k = AT^n \exp(-E/[RT])$. Units are mole, cm, s, cal.[8]

Number	Reaction	A	n	E
R-2.3	$N + NO \leftrightarrow O + N_2$	$9.4 \cdot 10^{12}$	0.140	0
R-2.4	$N + OH \leftrightarrow NO + H$	$3.8 \cdot 10^{13}$	0	0
R-2.5	$N + O_2 \leftrightarrow NO + O$	$5.9 \cdot 10^{9}$	1	6280

Another important source of NO is the denominated fuel NO, which is also highly dependent on the O/H radical presence where the concentration increases up to an equivalence ratio of 0.9. [5] It encounters a further decline when values of equivalence ratio increase towards rich combustion. Around 70% of NO production comes from the HNO intermediate, as shown in reaction R-2.6 to R-2.11, where R-2.10 becomes significant.

$$NH_2 + O \leftrightarrow HNO + H \quad \text{R-2.6}$$

$$NH_2 + OH \leftrightarrow HNO + H \quad \text{R-2.7}$$

$$HNO + M \leftrightarrow NO + H + M \quad \text{R-2.8}$$

$$HNO + H \leftrightarrow NO + H_2 \quad \text{R-2.9}$$

$$HNO + OH \leftrightarrow NO + H_2O \quad \text{R-2.10}$$

$$HNO + O_2 \leftrightarrow NO + HO_2 \quad \text{R-2.11}$$

Simultaneously, according to Peter Alborg, the presence HO_2 increases the formation of NO_2 and total oxidation of NO as seen in reaction R-2.12. [27]

$$NO + HO_2 \leftrightarrow NO_2 + OH \quad \text{R-2.12}$$

Even though the NH_3 and H_2 emissions are insignificant in the lean conditions, the NO concentrations are around 2000 ppm. [15] In terms of pressure, the principal consumption phase for ammonia remains unchanged as pressure increases, although pressure depletes the O/H radical pool. [13]

Burning under rich conditions minimizes NO_x compound production. [5] The formation of NO in the burning of an NH_3-air mixture reduces rapidly with an increasing equivalence ratio, especially after 1.05, becoming nearly zero at 1.1. [15] At the same time since N_2O has a warming potential of 300 times the CO_2, optimal circumstances appear to be near the equivalence ratio of 1.1, where both NO_2 and N_2O generated are minimal.[5] Furthermore, as the fraction of H in O/H radicals grows, the proportion of NH_x radicals increase in this kind of combustion, with the kinetic dominating reactions R-2.13, R-2.14 and R-2.15.

$$NH_3 + H \leftrightarrow NH_2 + H_2 \quad \text{R-2.13}$$

$$NH_2 + H \leftrightarrow NH + H_2 \quad \text{R-2.14}$$

$$NH + H \leftrightarrow N + H_2 \quad \text{R-2.15}$$

The most important dissociation event that leads to N_2 production without requiring NO is the bonding interaction of NH_x compounds that generate the intermediate NNH molecule. Figure 2.6 displays the most important reaction occurring in rich flames for the nitrogen species.

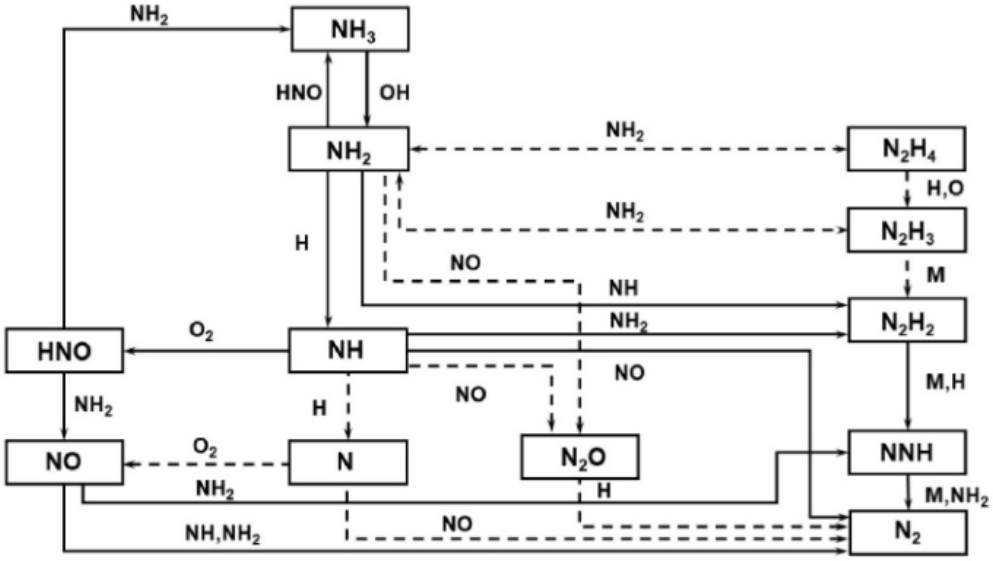

Figure 2.6: Important reaction paths of nitrogen species in rich ammonia flames. [5]

There are several numerical mechanisms in the bibliography that forecast ammonia combustion. While recognizing the generation of N_2H_3 and N_2H_4 from the NH_i radical combination steps, Konnov and De Ruyck incorporated the full N/H mechanism. [13] GRI Mech 3.0 closely predicts the measurements of the burning velocity shown in Figure 2.7, but as well as previous studies such as Miller and Bowman, Vandooren et al., and Lindstedt et al.; neglected some significant ammonia oxidation steps such as the NH_i radical combination and the $NH_2 + NO$ reactions in their investigations, which are important for NO concentration prediction. For its part, the Konnov mechanism overestimates the burning velocity.

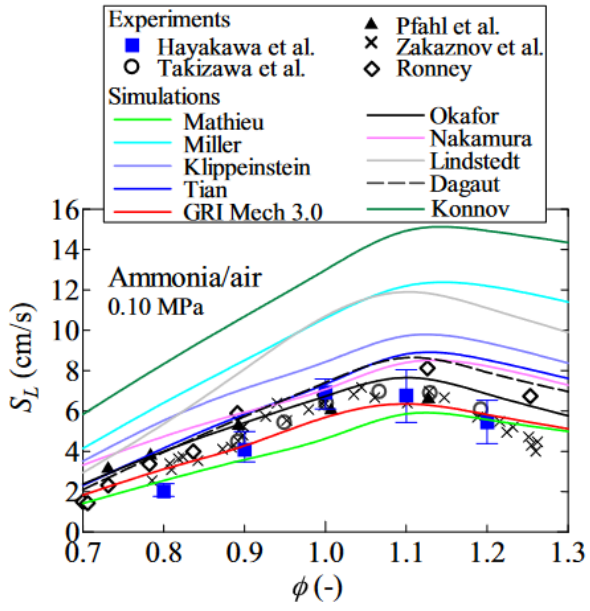

Figure 2.7: Comparison of the Kobayashi et al. measured burning velocity to the kinetic prediction models of Mathieu, Miller, Klippeinstein, Tian, GRI Mech 3.0, Okafor, Nakamura, Lindsted, Dagaut and Konnov at the mixture temperature of 298 K and 0.10 MPa of pressure. [13]

On the other hand, operating with an ammonia surplus at higher temperatures than 400 ºC and 1atm initiates the decomposition reaction, as shown in reaction R-2.16 which achieves a conversion of 99.99 while leaving trace quantities of unconverted ammonia. [28]

$$2NH_{3(g)} \leftrightarrow N_{2(g)} + 3H_{2(g)} \quad \text{R-2.16}$$

The breakdown is the inverse reaction of the Haber-Bosch ammonia production process. [29] The generated hydrogen is also combusted via a hydrogen-oxygen reaction mechanism, which has been extensively researched and has several applications, including high energy rocket engines. [30]

Finally, the alternative use of catalytic material can reduce the NO_x produced by the reduction of the chemical via a catalytic process over zeolites of reactions R-2.17 and R-2.18. [26]

$$4NO + 4NH_3 + O_2 \leftrightarrow 4N_2 + 6H_2O \quad \text{R-2.17}$$

$$6NO_2 + 8NH_3 \leftrightarrow 7N_2 + 12H_2O \quad \text{R-2.18}$$

2.3.4 Energy conservation equation

A simplified 1-D energy conservation equation can be derived by applying the first law of thermodynamics, Equation (2.12). [25]

$$Q - W = H_p - H_r + K_E + P_E \quad (2.12)$$

where Q represents heat entering/exiting the system, W represents work applied by or towards the system, K_E is the kinetic energy, P_E represents the potential energy, H_p and H_r are product and reactant enthalpies.

Given that the system operates in the steady-state and isobaric conditions, Equation (2.12) may be simplified as indicated in Equation (2.13).

$$H_r = H_p + Q \quad (2.13)$$

Equation (2.13) can alternatively be represented as Equation (2.14), and for simplicity, Equation (2.15) is obtained to compute the temperature attained by the products stream when the specific heat capacity (C_p) of product and reactants remain constant.

$$\Delta H = \int C_p dT \quad (2.14)$$

where ΔH denotes the change in enthalpy of the reactants and products, and dT denotes the change in temperature. The C_p at different temperatures is calculated using the Shomate equation and the constant values listed in Appendix B.

$$T_{out} = T_{in} + \frac{\Delta H_{rxn} - Q}{m_p \cdot C_p} \quad (2.15)$$

where T_{out} is the final temperature attained by the products in the combustor, T_{in} is the initial temperature, ΔH_{rxn} is the enthalpy of the reactions, derived as the difference between the formation enthalpies of the reactants ($\Delta h^0_{i,R}$) and products ($\Delta h^0_{i,P}$) involved in the reaction, as illustrated in Equation (2.16).

$$\Delta H_{rxn} = \frac{\sum(n_{i,R} \cdot \Delta h^0_{i,R} - n_{i,P} \cdot \Delta h^0_{i,P})}{m_{NH_3}} \quad (2.16)$$

where $n_{i,R}$ and $n_{i,P}$ are the number of moles of species i in the reactants and products, m_{NH_3} is the mass of NH_3.

Table 2.3 gathers the necessary information about the enthalpy of formation of the major substances, being the enthalpy of formation of a pure element is zero.

Table 2.3: Enthalpy of formation of the major species. [25]

Species	$\Delta\hat{h}^0$ (MJ/kmol)
H_2O	-241.83
NH_3	-46.2
NO	90.29
NO_2	33.1

The heat transmitted (Q_T) to the surroundings is estimated using Fourier's law, Equation (2.17) [31]

$$Q_{cond} = \frac{kA(T_{w1} - T_{w2})}{L} \quad (2.17)$$

where k is the thermal conductivity in W/mK, A is the transmission area in m^2, T_{w1} is the temperature of the internal wall, T_{w2} is the temperature of the insulator and L is the thickness.

The transmission area for the heat loss will depend on the geometry of the combustor, which consists of a cylindrical geometry as Equation (2.18).

$$A = \pi d h_c + \pi \frac{d^2}{4} \quad (2.18)$$

The maximum theoretical temperature of the flame is obtained when there is no heat loss in the GCU, meaning that the combustor operates under adiabatic circumstances as shown by Equation (2.19). [25]

$$T_{ad} = T_{in} + \frac{\Delta H_{rxn}}{m_p \cdot C_p} \quad (2.19)$$

The mass of products can be correlated to the mass of the reactants through the mass conservation equation and the fuel-air ratio parameter from Equation (2.1), as seen in Equation (2.20).

$$m_p = m_a \left(1 + \frac{m_a}{m_f}\right) \quad (2.20)$$

2.3.5 Flame speed

The flame speed is the rate of propagation of the flame into the unburned mixture in a combustion reaction. [25] The primary distinction may be made by the classification of the flame as premixed and non-premixed flames. Premixed flame is the scenario where oxygen is fuel are previously mixed and non-premixed flames are also known as diffusion flames. Both

of them can be considered laminar or turbulent flames depending on the fluctuating motion of the fluid. The study of the speed of laminar and turbulent flames is challenging since the flame is a dynamic object, but necessary because it may be used for verifying chemical models. [32] [33] Each fuel has a distinct propagation speed and the laminar flames are in many combustion models the base for the calculation of the turbulent flames. [32] It has been observed experimentally that turbulent flames have a faster propagation speed than their laminar counterparts, they can propagate up to two orders of magnitude faster. [25] Figure 2.8 shows the temperature, compositions and speed structure of a premixed laminar flame. The reaction zone is where the reaction takes place and the adjacent zone, preheated zone, is where the flame supplies heat upstream to the unburned mixture. [33]

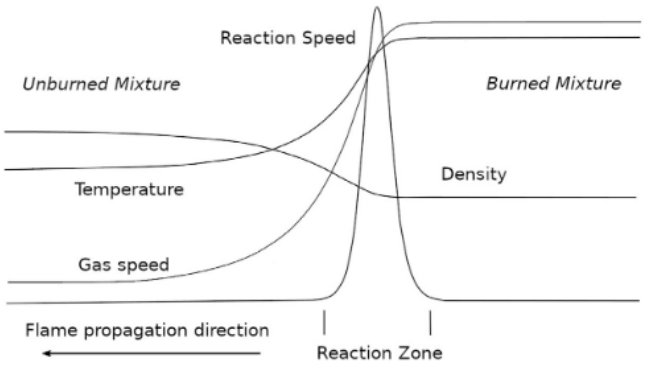

Figure 2.8: Premixed Laminar flame structure, where the abscissa axis normally represents the distance in the flame. [33]

Figure 2.9 illustrates a diffusion flame with the reaction occurring on the surface of the flame and the products reaching the temperature of the products (T_p) due to the lack of oxidizer inside the flame. [25]

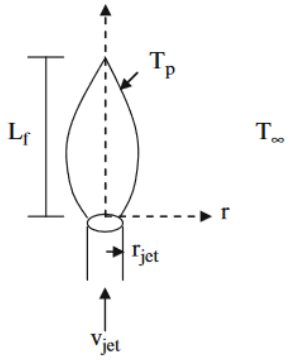

Figure 2.9: Typical diffusion flame structure. Where L_f is the laminar flame height, r_{jet} is the radio of the nozzle, v_{jet} is the velocity of the fuel through the nozzle and T_∞ is the temperature of the surroundings.

There are several methods to compute the structure of a laminar flame, depending on the chemistry and transport complexity. [32] Flame speed calculations of complex systems require numerical solutions. As a result, Equations (2.24) and (2.22) may be used to calculate the flame thickness (δ), which is made up of the preheated zone and the reaction zone. [25]

$$T_{10\%} = T_r + 0.1(T_p - T_r) \tag{2.21}$$

$$T_{90\%} = T_r + 0.9(T_p - T_r) \tag{2.22}$$

where $T_{10\%}$ is the point at which the temperature has risen 10%, $T_{90\%}$ is the point at which 90% of the temperature has risen, T_r and T_p are the temperatures of reactants and products.

By using Equation (2.23) the chemical time scale (τ_{chem}) is determined.

$$\tau_{chem} \approx \frac{\delta}{S_L} \tag{2.23}$$

where $S_L$is the laminar burning velocity.

Turbulent flame speed (S_t) may be calculated using Equation (2.24) where the German chemist Damköhler assumed that turbulent flame speed should be proportional to the area of the surface of the corrugated laminar flame for the large-scale lower-intensity turbulence. [33]

$$S_t = S_L \frac{A_L}{A_{average}} \tag{2.24}$$

where A_L is the total surface area of the laminar flame and $A_{average}$ is averaged over the time area of the turbulent flame.

In practice, through the continuity equation, the average flame speed (u) for the experiments, is calculated by the relationship between the area from which the gas flows and the volumetric flow as shown in Equation (2.25). [25]

$$u = \frac{\dot{V}_R}{A} \tag{2.25}$$

where u is the average burning velocity of the unburned mixture, $\dot{V}_R$ is the volumetric flow rate of the reactants obtained by the ideal gas law and A is the area of the pipe.

For a diffusion flame, by using geometric relations the flame speed can be determined by equation (2.26).

$$S_L = u \cdot sin(\alpha) \tag{2.26}$$

Equation (2.27) offers the expression for calculating the laminar burning velocity of ammonia at temperatures other than room temperature. [34]

$$\frac{S_L}{S_L^0} = \left(\frac{T_u}{T_u^0}\right)^{\alpha} \tag{2.27}$$

where $S_L$is the laminar burning velocity at the unburned temperature (T_u) and S_L^0 is the laminar burning velocity at room temperature (T_u^0).

3 Experimental methodology

This chapter includes important considerations for setting up the experimental equipment and doing the experimental task. The tests are centered on burning ammonia in rich mixture conditions, especially in the 0.9-1.1 range of equivalence ratio. The experimental circumstances are further used to calculate the simulation parameters.

3.1 Experimental setup

The experiments are conducted in a Wärtsilä-design high swirl premix burner with a recirculation zone to guarantee flame stabilization.

The primary equipment, which consists of a refractory conical burner encircled by a metallic insulated cylindrical combustion chamber with a tiny quartz glass window, is connected to two ammonia-pressurized containers. The ammonia is first delivered to the premix unit pipe, where it is combined with air. A centrifugal fan previously propelled the air. The premix unit, which is connected to the combustion chamber at the top allocates a swirler, shown in Figure 3.1, that is strategically placed to assist stabilize the flame in the burner, as illustrated in Figure 3.2. Inconel 939, a high-temperature nickel super-alloy, is used to make the 3D-printed propeller. The propeller unit is made up of 12 vanes with a 44º angle and a 60 mm core internal diameter. The burner, which also stabilizes the flame and shields the inlet region from flame exposure, has an internal diameter of 110 mm and is made of 60% alumina/30% silicate mullite-based castable cement, its dimensions are illustrated in Figure 3.3. [35]

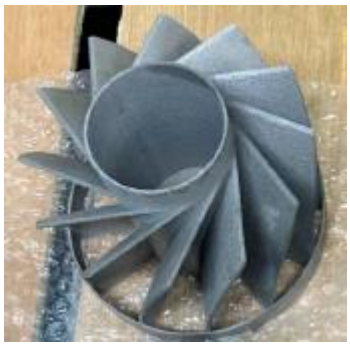

Figure 3.1: 12-60-44 propeller. [35]

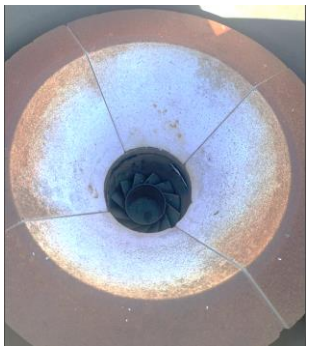

Figure 3.2: Swirler and cone setup.

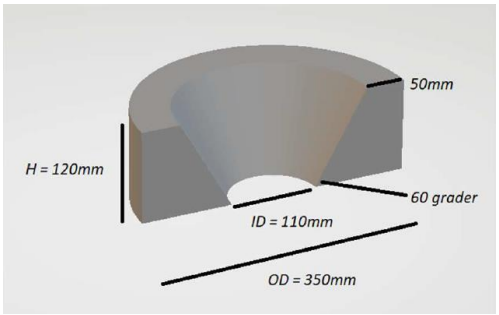

Figure 3.3: Dimensions of the cone burner. [35]

A high-energy exciter is installed on the side of the combustion chamber perpendicular to the premix unit to manually ignite the mixture. Some ammonia indicators and thermocouples for temperature measurement at various points in the process are provided. Figure 3.4 depicts the

process flow diagram of the system, whereas Figure 3.5 displays the sustained combustion chamber with the premix unit at the bottom and the ignition stick on the side.

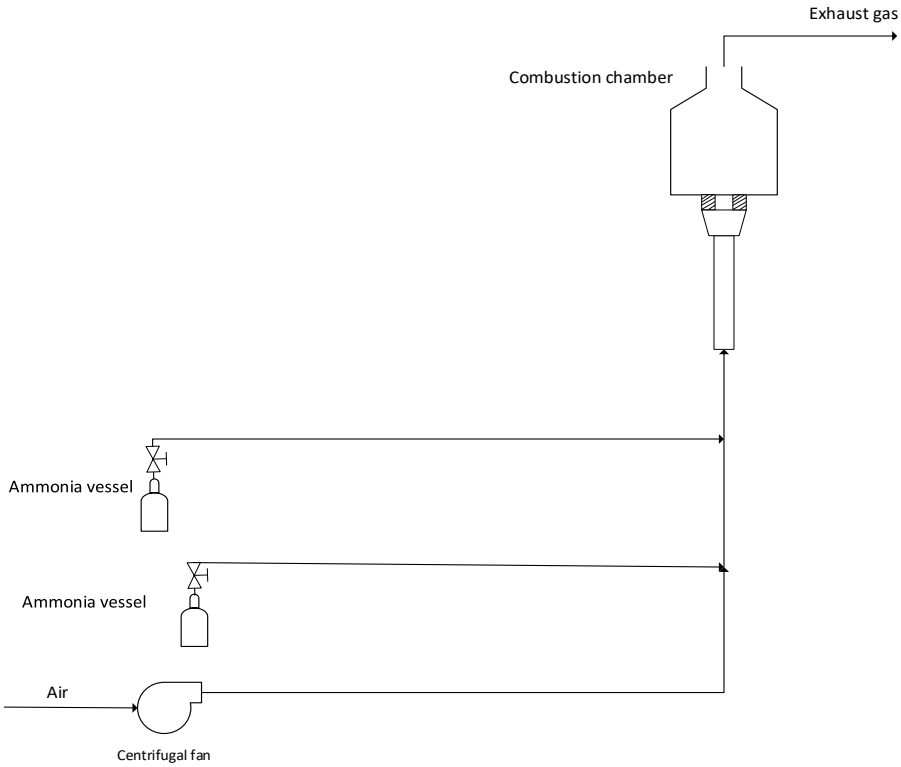

Figure 3.4: Process flow diagram of the experimental setup.

Figure 3.5: Experimental setup of the gas combustor unit.

Finally, a Testo 350 analyzer is used to measure the NO_x components in the exhaust stream.

Two different experiments were carried out and the considerations are summarized in

Table 3.1.

Table 3.1: Experimental conditions.

	Experiment 1	**Experiment 2**
Fuel	Ammonia	Ammonia
Nitrogen vent gas	Yes	No
Oxidizer	Air	Air
Phase	Gas	Gas
Flame stage 1	Premix	Premix
Covering stage 1	Cylindrical	Cylindrical
Insulation material	SuperMag	SuperMag
Thickness insulation [mm]	26	26
Flame stage 2	Diffusion	Diffusion
Covering stage 2	No	Yes
NO_x measurement	No	Yes

3.2 Procedure experiment 1

The combustion unit of experiment 1 is a two-stage burner as depicted in Figure 3.6. The premix NH_3-air mixture is burnt in the first step. When working under rich fuel conditions and temperatures higher than 400 ℃, the excess NH_3 decomposes into hydrogen which is burnt in the second stage. At a certain moment, N_2 is also delivered directly into the combustion chamber through different inlets. The overall dimensions of the combustion chamber are shown in Figure 3.7, where the cylindrical vessel has a diameter of 460 mm and a total height of 750 mm. The exit nozzle has a diameter of 70 mm. Figure 3.8 illustrates the process flow diagram for this experiment.

The experiment began by opening the valves of one of the NH_3 containers and the mixture was ignited and stabilized after a few seconds. To achieve the appropriate equivalence ratio, the ammonia and air mass flows are increased gradually. Nitrogen is later injected for a few seconds. Temperature, pressure and mass flow measurements are collected in a control panel.

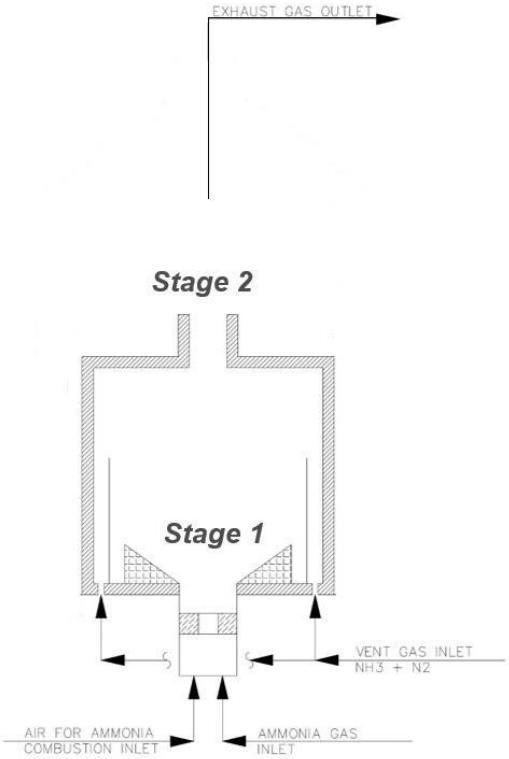

Figure 3.6: Sketch of the combustion chamber in experiment 1. [36]

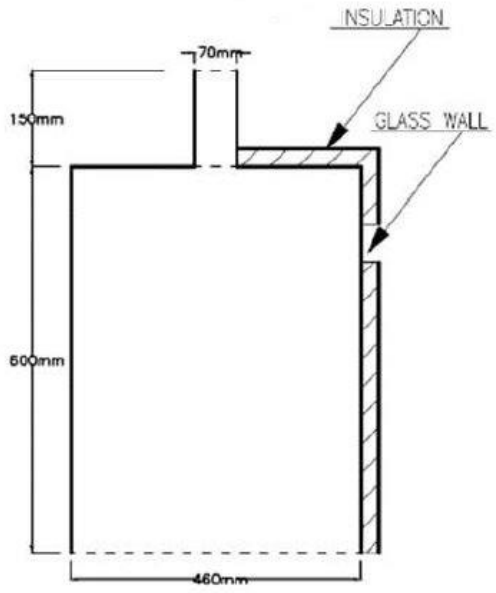

Figure 3.7: Dimensions of the combustion chamber. [37]

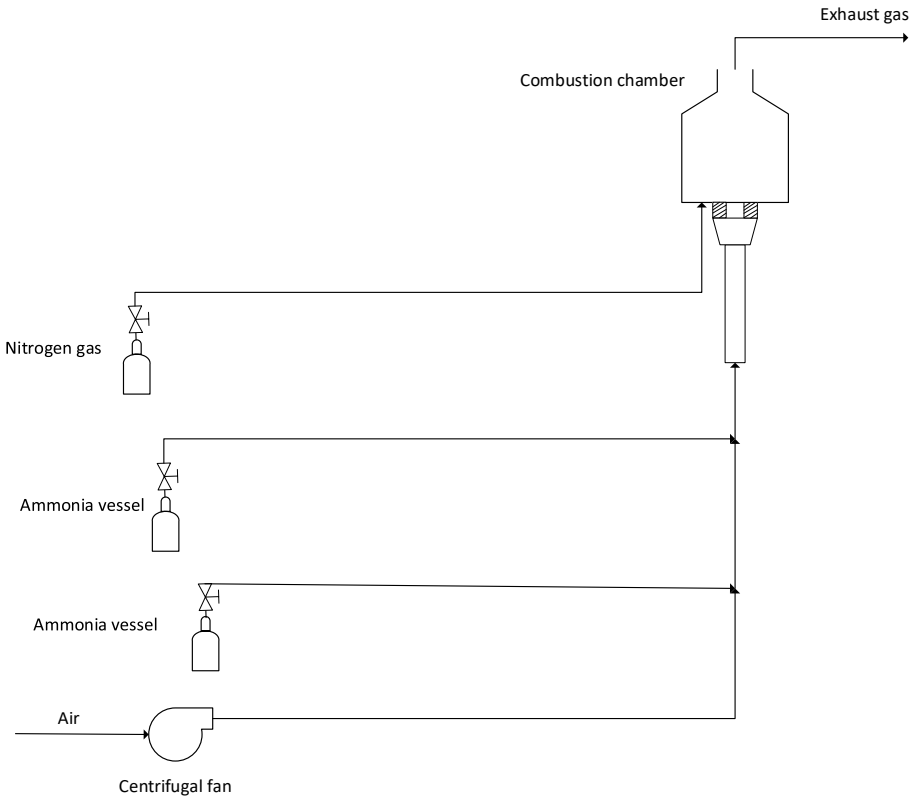

Figure 3.8: Process flow diagram for the experimental setup 1.

3.3 Procedure experiment 2

The combustion unit of experiment 2 is similar to the previous two-stage burner. However, the second stage of this arrangement is covered by another cylindrical metallic structure with a small quartz glass window, through which air is introduced to assist with the combustion of the hydrogen flame and dilute the exhaust gas composition, so the temperature of the output is below 450 ℃. In this experiment, nitrogen gas is not used at any point in time, and the amount of NO_x present in the exhaust gas composition is measured. The steps are the same as in experiment 1.

A sketch of the experimental unit is depicted in Figure 3.9. The dimensions and locations of the thermocouples are illustrated in Figure 1 in Appendix C, where the cylinder of the first stage has the same dimensions as in experiment 1, and the structure of the second stage which can be divided into a cone and cylinder, has a diameter of 400 mm. The height of the cylinder is 350 mm, and the cone has an angle of 45^o and an outlet nozzle of 84 mm. Finally, the process flow diagram is shown in Figure 3.10.

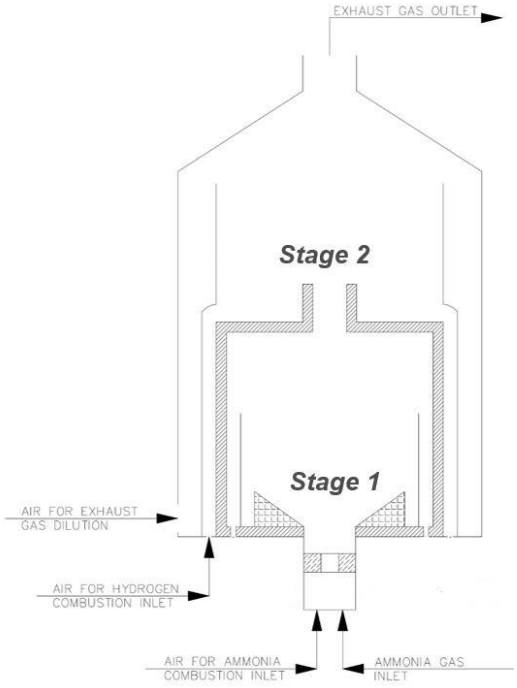

Figure 3.9: Combustion chamber and burner of the experimental setup 2. [36]

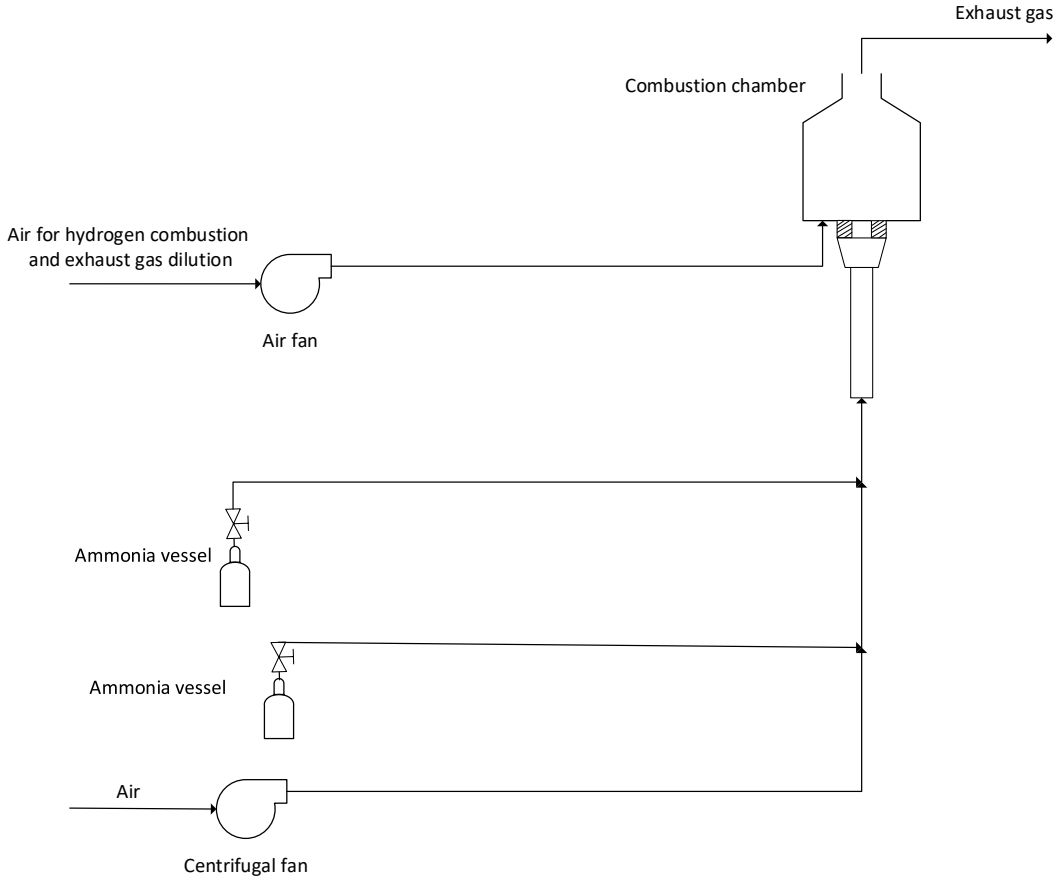

Figure 3.10: Process flow diagram for the experimental setup 2.

4 Simulation methodology

The simulations are conducted by using numerical techniques on the Cantera software version 2.6. Konnov is the mechanism used for comparing experimental data with the simulation behavior of stage 1 for ammonia combustion because of its more detailed treatment of ammonia chemistry. [38] [39] The complete mechanism includes more than 85 species and 1200 reactions for C, H , N and O elements. [38] The Gri 3.0 mechanism, which is firmly established and primarily used for simulating natural gas flames, also considers some nitrogenous species, and it is included as a reference mechanism. Both methods will be employed in a simplified form that does not include the C compounds. The h2o2 method is used to simulate hydrogen combustion, even though the Konnov mechanism is equally acceptable. [33]

The simulations are conducted for the experiment 1 data in Table 4.1 by using the freely-propagating, adiabatic 1D flame module to calculate the laminar burning velocity; since the laminar burning velocity is the reference for combustion studies. [32] As a result, the steps listed below are taken for the temperature of 400 K and pressure of 1 atm:

1. Set the initial conditions of the unburned mixture, such as temperature, pressure equivalence ratio and composition. All the simulations are carried out at atmospheric pressure to replicate the experimental conditions.
2. Set the width of the domain in which the flame ought to be solved.
3. Calculate the burning velocity and composition of the flame.
4. Perform a sensitivity analysis to observe what reaction affects the most to the mechanism.

Table 4.1: Simulation data from experiment 1, where $\dot{n}$ is in mol/s and $\dot{n}_{N_2}$ is the molar flow rate of vent N_2.

$\boldsymbol{\phi}$	$\dot{\boldsymbol{n}}_{\boldsymbol{NH_3}}$	$\dot{\boldsymbol{n}}_{\boldsymbol{N_2}}$	$\dot{\boldsymbol{n}}_{\boldsymbol{O_2}}(\boldsymbol{air})$	$\dot{\boldsymbol{n}}_{\boldsymbol{N_2}}(\boldsymbol{air})$
0.901	0.130	0.020	0.107	0.411
0.907	0.082	0	0.067	0.255
0.915	0.130	0.337	0.106	0.405
0.965	0.098	0	0.075	0.288
0.970	0.098	0	0.075	0.286
0.971	0.114	0	0.087	0.334
0.994	0.130	0	0.097	0.373
0.000	0.000	0	0.000	0.000
1.005	0.098	0	0.072	0.277
1.008	0.114	0	0.084	0.322
1.019	0.130	0	0.095	0.364
1.027	0.147	0.347	0.106	0.406
1.030	0.098	0	0.070	0.270
1.054	0.163	0	0.115	0.439
1.061	0.114	0	0.080	0.306
1.075	0.163	0	0.113	0.431
1.080	0.130	0	0.090	0.343
1.100	0.130	0	0.088	0.337

The NO_x composition in the burned mixture was obtained with the Cantera equilibrate command considering there is no change in pressure. The NO_x composition is obtained at the corresponding adiabatic flame temperature for each equivalence ratio.

5 Results

The outcomes of the tests and simulation segments are summarized in this chapter. It focuses on the assessment of the recorded and estimated temperatures, the heat flows of the flame and through the reactor, the laminar and turbulent flame velocities and sensitivity analysis.

5.1 Experimental temperature profiles

First, the temperature of the flames in each stage, ammonia and hydrogen, was estimated by using the equation (2.19) and plotted with the temperature recorded in the combustion unit and the ammonia flame as illustrated in Figure 5.1 and Figure 5.2.

According to the temperature profiles in Figure 5.1, the NH_3 flame temperature is roughly 50% of the estimated adiabatic flame temperature. The temperature in the combustion unit, on the other hand, follows a similar pattern to that of the NH_3 flame temperature measured. The expected H_2 adiabatic flame temperature, it is essentially 1% higher than the predicted temperature for the NH_3 component in non-adiabatic conditions, mainly the stage 1 outlet stream. Finally, the measured H_2 flame temperature profile displays a significant fluctuating trend and is the lowest recorded.

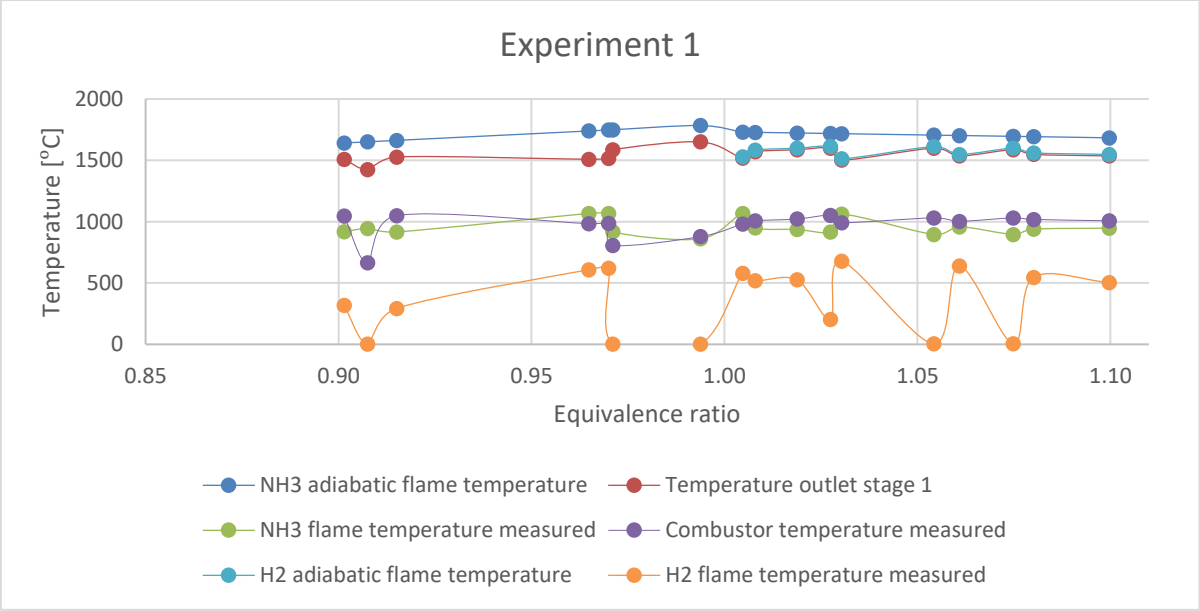

Figure 5.1: Temperature profiles of experiment 1.

Figure 5.2 for its part indicates that the recorded NH_3 flame temperature is roughly 15% of the estimated NH_3 adiabatic flame temperature. The predicted outlet stream temperature of stage 1 is approximately 80% of the anticipated adiabatic flame temperature of NH_3. The stage 1 combustion unit temperature is somewhat higher than the NH_3 flame temperature which may be up to 40% higher in the rich combustion. In this situation, the predicted adiabatic flame temperature of the H_2 is 1% higher than the stage 1 output temperature. Furthermore, the measured temperature of H_2 is around 15-20% of the predicted H_2 adiabatic flame temperature. The output temperature of stage 2 is above 500 ℃ for the lean and rich conditions, except for the equivalence ratio of 1.06 which reach a temperature of 492 ℃.

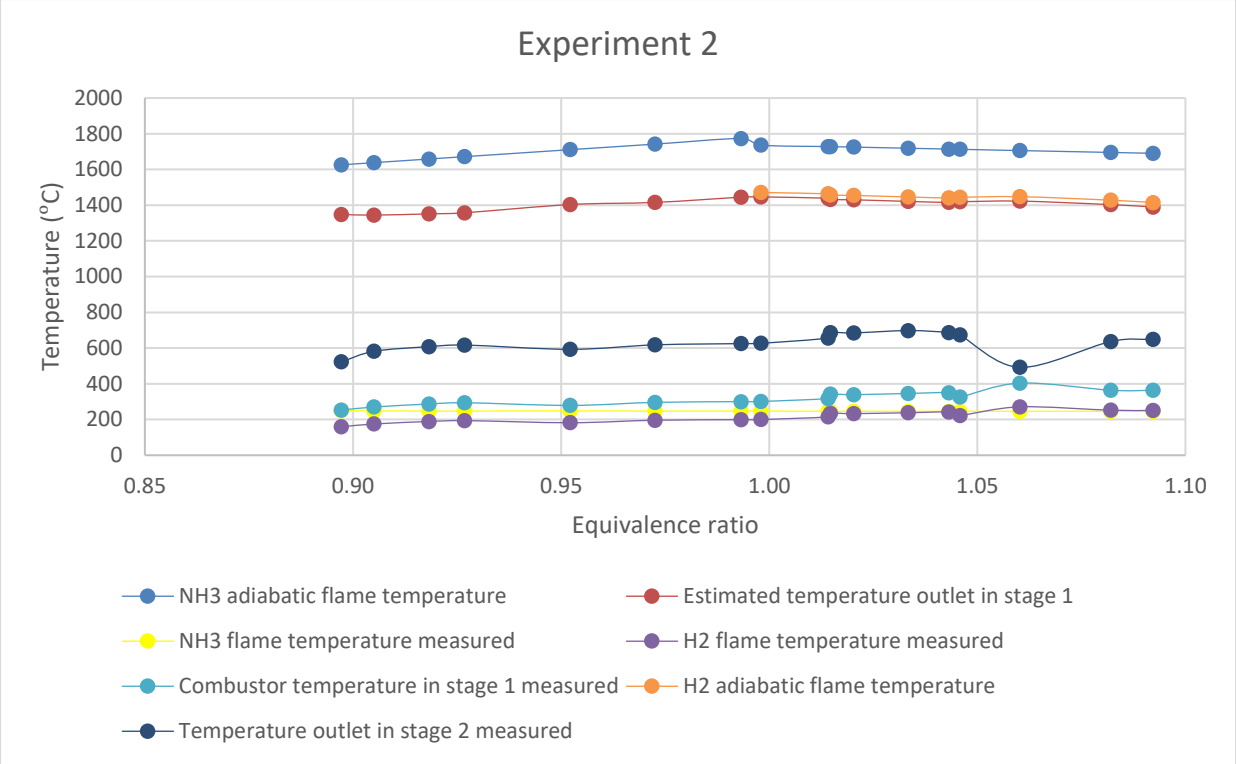

Figure 5.2: Temperature profiles of experiment 2.

5.2 Heat release of the experiments

The heat loss to the surroundings was estimated with equation (2.17). For both experiments, the heat of conduction through the insulator for the first stage of the combustion unit was examined.

Figure 5.3 depicts the heat of the reaction produced by ammonia combustion and the heat lost to the environment for experiment 1, with the former being roughly 39% for lean combustion and somewhat lower, 32%, for rich conditions. Moreover, the heat loss is more stable in the rich combustion section. The ammonia low heating value profile fluctuates and contains several minimums and maxima, examples are for an equivalence ratio of 0.907 with the heat of reaction of 23.1 kW and 30.6 kW for an equivalence ratio of 1.03. The heat of reaction for the stage 2, mainly the combustion of hydrogen, represents 1% of the heat of the reaction of ammonia and up to 9 % for more concentrated compositions of the rich spectrum as for the equivalence ratio of 1.1.

Figure 5.4 shows a somewhat larger heat loss for lean combustion, reflecting an average of 67% of the lower heating value, and a 62% heat loss for rich combustion. The greatest production of the heat of reaction in hydrogen is for the equivalence ratio of 1.09, which has a heat of reaction of approximately 4.6 kW.

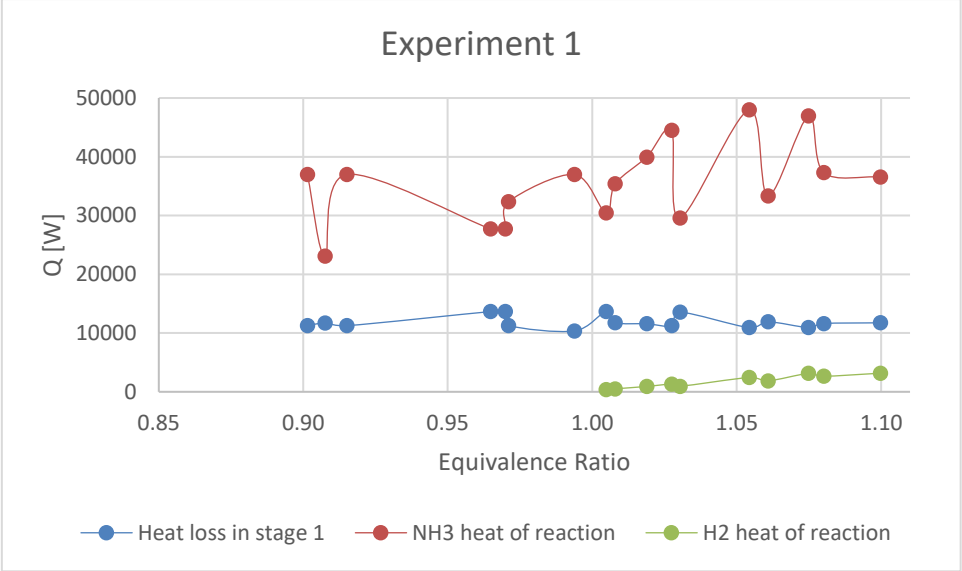

Figure 5.3: Heat flows in the combustion unit for experiment 1.

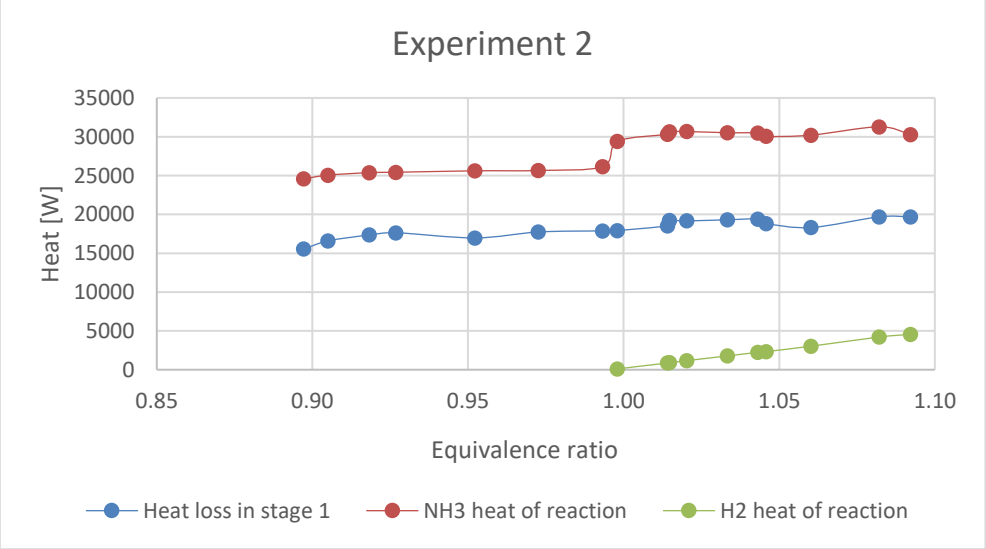

Figure 5.4: Heat flows in the combustion unit for experiment 2.

5.3 Hydrogen generation

For the rich premix mixtures, the production of H_2 was evaluated and estimated using the equilibrium reaction R-2.16 of NH_3 decomposition. Figure 5.5 shows ascending profiles for both trials when the equivalence ratio is increased. Experiment 1 produces more ammonia with 0.0224 at the equivalence ratio of 1.1. At the equivalence ratio of 1.09, the largest quantity of H_2 generated in experiment 2 is 0.0196.

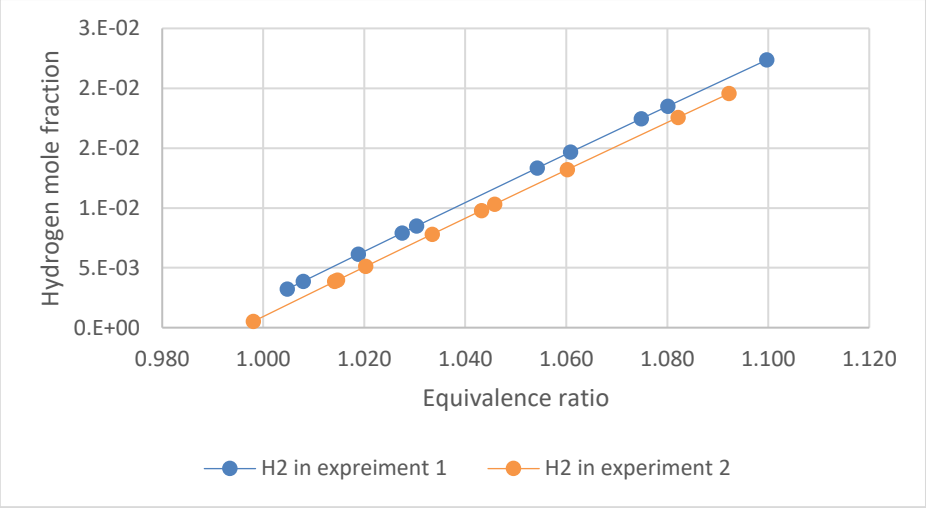

Figure 5.5: Hydrogen mole fraction generated in the experiments.

5.4 Flame speed

Figure 5.6 and Figure 5.7 show the turbulent flame velocity estimated with Equation (2.25) for both experiments, as well as the unburned speed of the gases at 300 and 400 K. Figure 5.6, shows the changing behavior of the speed profiles for experiment 1. Three distinct maxima are located in the profiles, corresponding to equivalence ratios of 0.901, 0.915 and 1.027. Extra N_2 was supplied into the combustion unit at certain times. The greatest speed figure for lean combustion corresponds to an equivalence ratio of 0.915 for the three profiles, which is 12.4 m/s for unburned gases at 400 K, i.e. 39% higher than its corresponding value at 300 K. Rich combustion has comparable performance, with a speed of 12.8 m/s for an equivalency ratio of 1.027. At 300 K, the unburned gas velocity ranges between 1.8 and 5 m/s. The flame speed profile has the lowest speed interval ranging from 0.8 to 1.8 m/s.

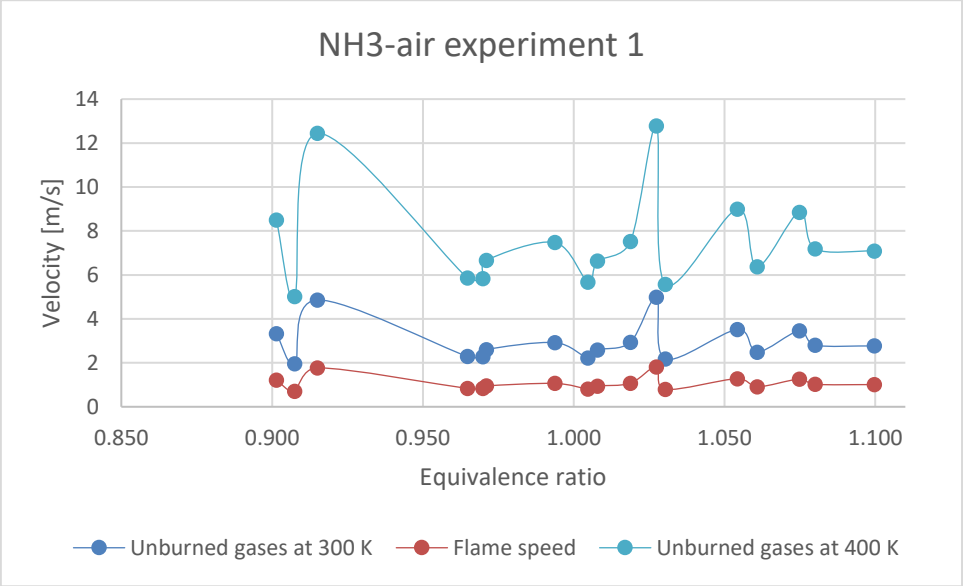

Figure 5.6: Velocity profiles for NH_3-air combustion in stage 1 for the experiment 1.

Figure 5.7 also shows more stable profiles. No vent N_2 was added at any point in this experiment. At 400 K, the unburned gases have a velocity range of 5.2 to 5.8 m/s, which is 39% greater than the unburned speed of the gases at 300 K. The former is close to 2 m/s. The

flame speed profile is less than 1 m/s, with the greatest value of 0.84 m/s for rich combustion at an equivalency ratio of 1.08.

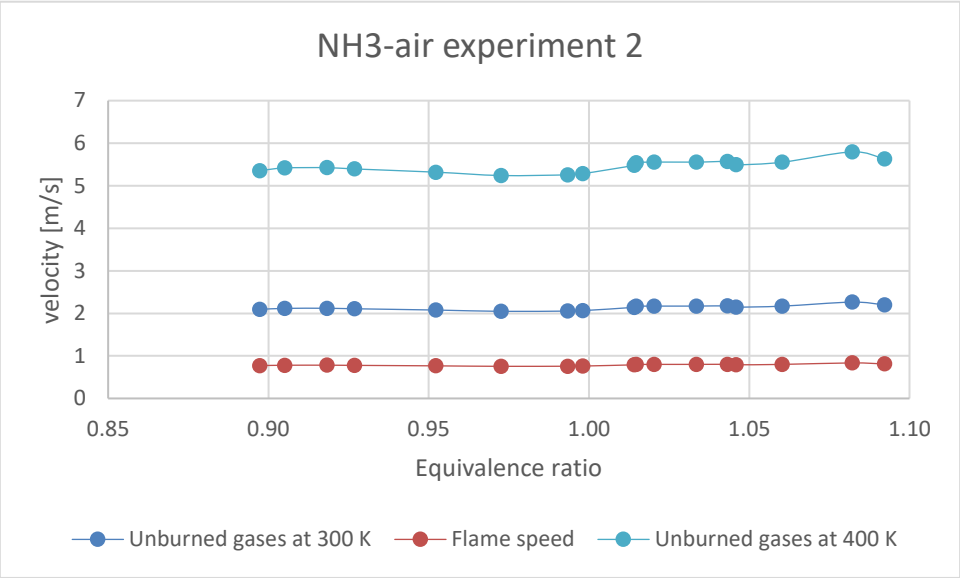

Figure 5.7: Velocity profiles for NH_3-air combustion in stage 1 for the experiment 2.

Figure 5.8 depicts the laminar flame velocities calculated by simulations to compare the model effects. Because vent N_2 was introduced at different points in time, it was determined to imitate the laminar burning velocities for experiment 1. Simulations are performed at 400 K to simulate the fact that heat diffusion will occur towards the reactants, causing the temperature of the reactant to be higher than 300 K when it enters the burner. At an equivalence ratio of 1.08, both mechanisms exhibit rising profiles that achieve the maximum flame speed. The Konnov mechanism achieves higher flame speed velocities with intervals of 11 to 14.6 cm/s, while the Gri 3.0 mechanism has an internal from 7 to 10.9 cm/s.

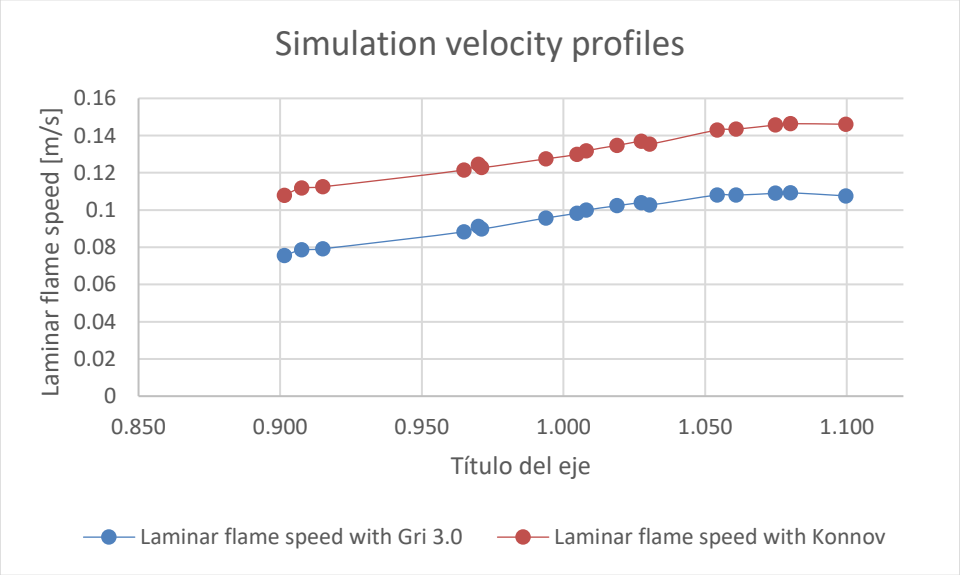

Figure 5.8: Laminar flame velocities (S_L) of NH_3 with Gri 3.0 and Konnov mechanisms at 400 K.

Figure 5.9 depicts the velocities of the stage 2 burner, which corresponds to the hydrogen velocity. They were estimated using the premises of reaction R- 2.16, in which the gas is mostly composed of H_2O and H_2. The unburned gases and flame speed profiles exhibit a similar oscillating pattern, in contrast to the more steady laminar flame speed profile. The gases depart

stage 1 combustion and enter stage 2 with velocities ranging from 14.8 m/s to 25 m/s. The flame speed, which is 42% slower than the unburned gases, ranges from 8.6 to 14.5 m/s, whereas the laminar flame speed ranges from 1.86 m/s for an equivalence ratio of 1 to 2.29 m/s for 1.1.

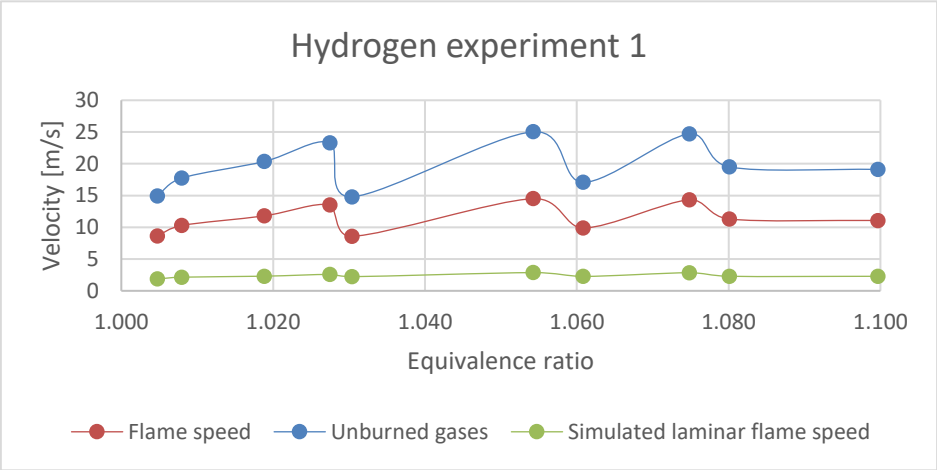

Figure 5.9: Velocity profiles for H_2-air combustion in the stage 2 for the experiment 1.

The evaluation for experiment 2 is depicted in Figure 5.10, which shows stable trends for both speed profiles and a minimum at the equivalence ratio of 1.06. Unburned gases achieve speeds ranging from 9.24 to 11.7 m/s, whereas flame speeds range from 5.96 to 6.79 m/s.

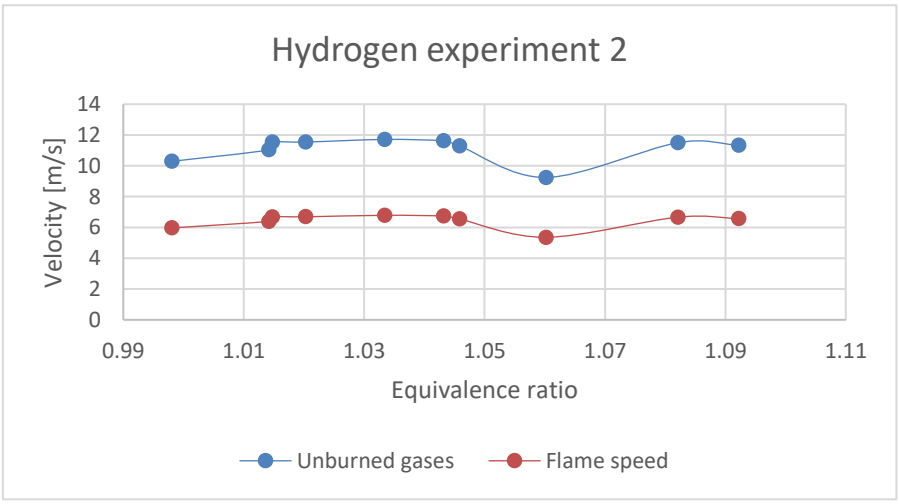

Figure 5.10: Velocity profiles for H_2-air combustion in the stage 2 for the experiment 2.

5.4.1 Premixed flame structure

Figure 5.11, Figure 5.12 and Figure 5.13 demonstrate the premixed flame structure for lean and rich combustion, respectively. The amount of NH_3 in the exhaust stream was essentially zero for both lean and rich settings. It was also noticed throughout the experiments since the ammonia detectors read 0 or 1 ppm, especially during the rich combustion configuration.

Figure 5.11 and Equations (2.21)-(2.23) show that for an initial temperature of 300 K and final temperature of approximately 2030 K, the flame thickness (δ) is 0.23 cm and chemical time (τ_{chem}) is 20.4 ms for a 0.915 equivalence ratio. Figure 5.12 depicts all of the primary component compositions along the flame for the previously given equivalency ratio. NO and H_2 are generated in small amounts but H_2 reacts instantly. N_2O and NO_2 are essentially zero.

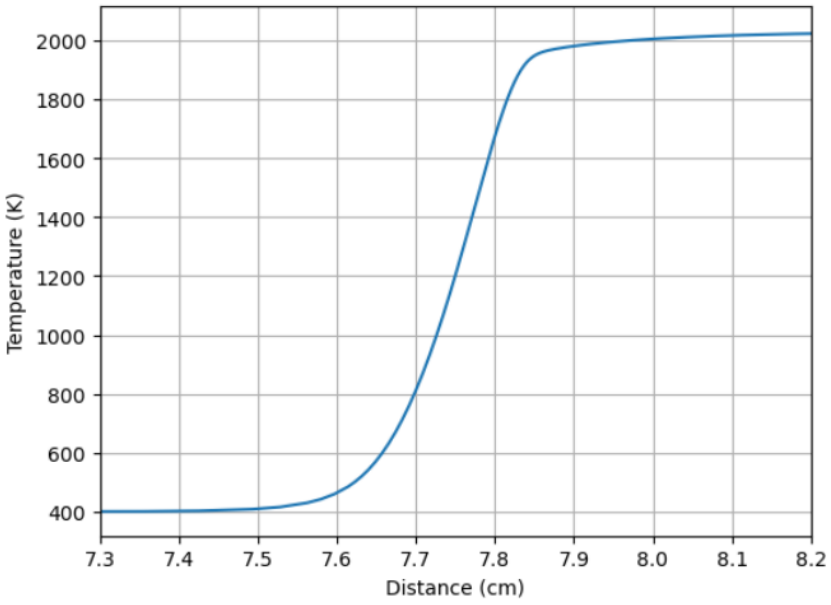

Figure 5.11: Temperature profile in the flame for an equivalence ratio of $\phi = 0.915$.

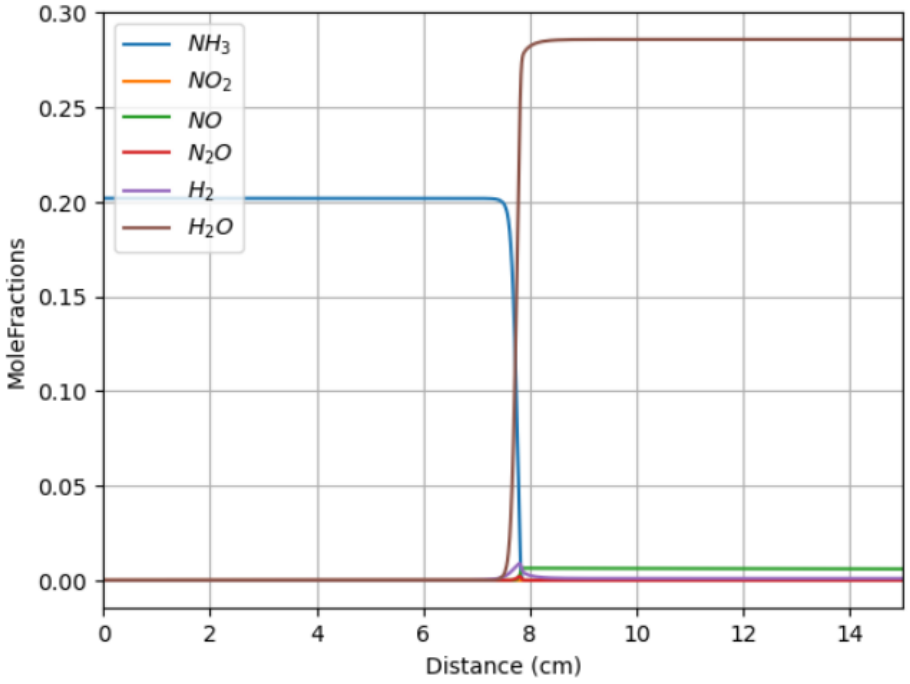

Figure 5.12: Profile compositions in the flame for lean combustion, mainly $\phi = 0.915$.

In the same manner, but with a temperature profile similar to Figure 5.11, an equivalence ratio of 1.1 has a flame thickness of 0.17 cm and a chemical time of 11 ms. In this situation, as in the rest of the rich combustions, the quantity of H_2 produced is greater and does not react immediately. The amount of NO generated is reduced. As in lean combustion, N_2O and NO_2 are almost non-existent.

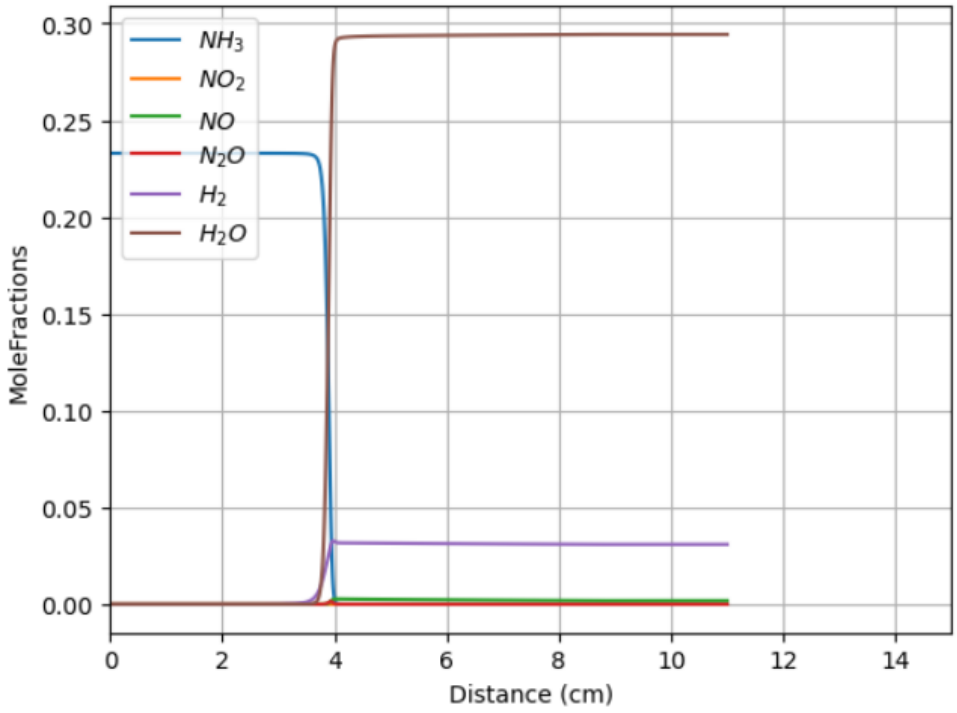

Figure 5.13: Profile composition in the flame for rich combustion, $\phi = 1.1$.

5.4.2 Flame speed sensitivity analysis

A sensitivity analysis was carried out with both mechanisms to identify the importance of the elementary reactions in the structure and propagation of the ammonia flame speed. In both Figure 5.14 and Figure 5.15, it is shown that the main reaction to accelerate the propagation of the flame speed is the radical reaction $H + O_2 \leftrightarrow O + OH$. The reactions with a negative sensitivity coefficient can inhibit flame propagation.

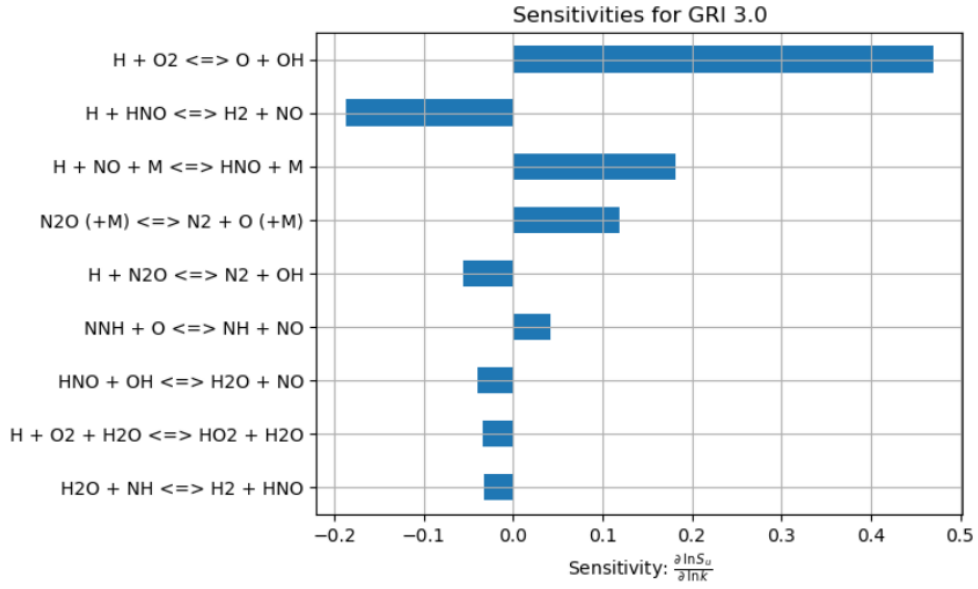

Figure 5.14: Sensitivity analysis of the flame speed with the Gri 3.0 mechanisms.

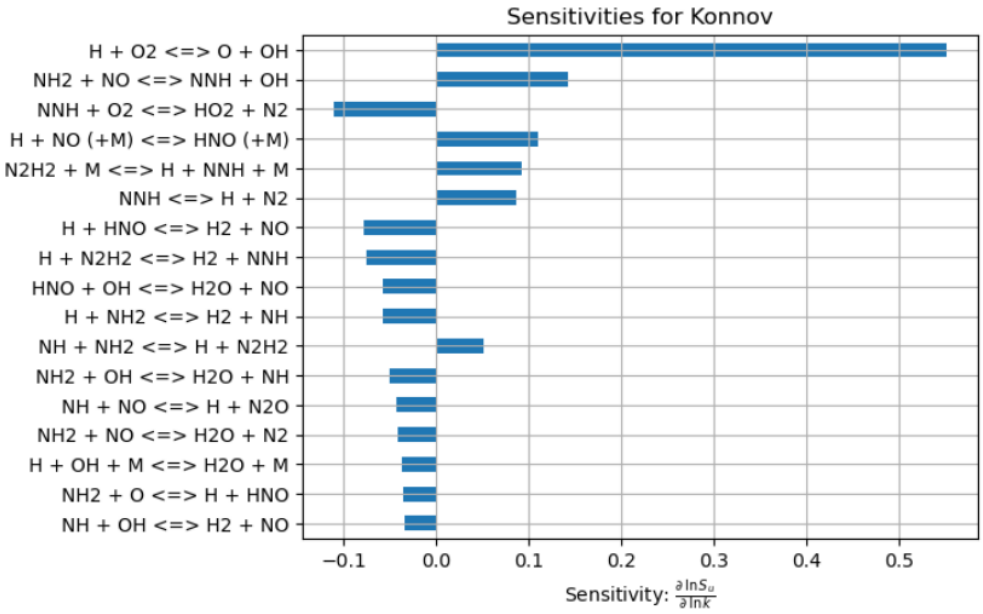

Figure 5.15: Sensitivity analysis of the flame speed with the Konnov mechanisms.

5.5 NOx emissions

Theoretical NO_x emissions were estimated using reaction R-2.2, where NO is the primary component of nitrous oxides generated. Figure 5.10 depicts the NOx emissions measured using the TESTO equipment as well as the calculated with reaction R-2.2. Experiment 1 had the highest emissions, with about 130000 ppm and variable behavior. For the lean circumstances in experiment 2, the profile is steadier and has an upward trend with a higher equivalence ratio. The emission data measured with the equipment is labelled experimental and is close to zero.

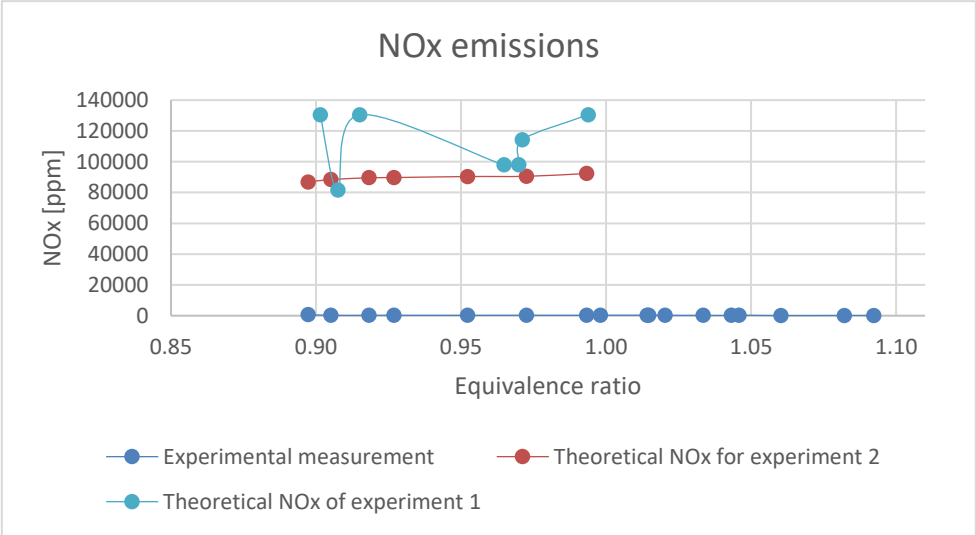

Figure 5.16: Theoretical and experimental NO_x emissions.

Figure 5.17 depicts how the simulated emissions decrease as the equivalence ratio increases. Furthermore, for lean combustions, the emissions are about $1.5 \cdot 10^6$ppm. The theoretical emissions are the same as those estimated in experiment 1 with reaction R-2.2.

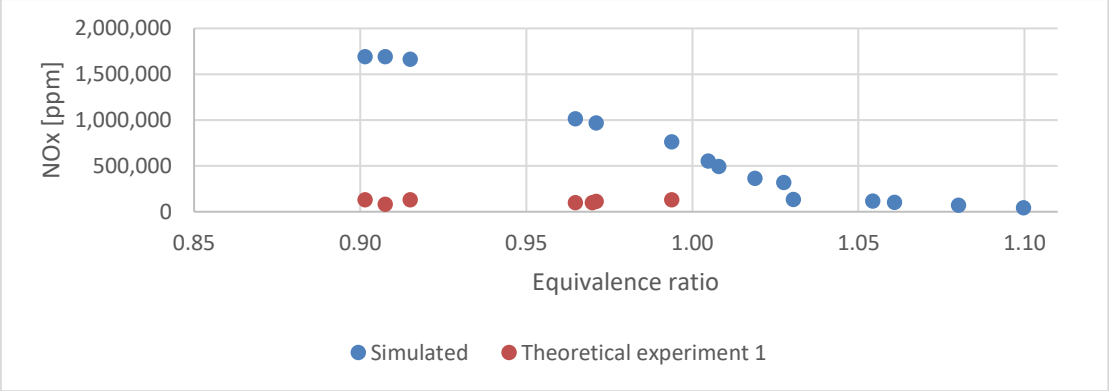

Figure 5.17: Comparison of simulated NO_x emission with the theoretical emissions.

Figure 5.18 illustrates which fraction of NO_x observed in experiment 2 is NO and which is NO_2. The largest quantity of NO is found at the equivalence ratio 0.9 with over 700 ppm and declines with increasing equivalence ratio. The least amount is found at an equivalence ratio of 1.06 with 57 ppm emissions. In both lean and rich circumstances, NO_2 emissions are essentially non-existent with 16 ppm.

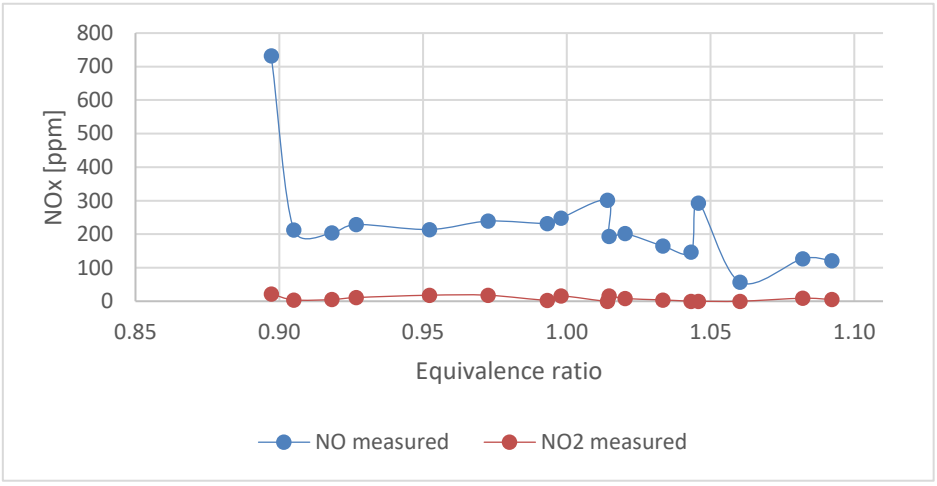

Figure 5.18: Proportion of NO and NO_2 emission measured with the TESTO equipment in experiment 2.

5.6 Discussions

The recorded NH_3 and H_2 flame temperatures are much lower than the adiabatic flame temperature in both tests due to heat loss from the combustion unit, which is up to 39% in the first experiment and 67% in the second experiment. Rich NH_3-air premix mixtures demonstrated lesser heat loss, with 32% for experiment 1 and 62% for experiment 2. The increased heat loss in experiment 2 is caused by its upper surface not being surrounded with the SuperMag isolation material and instead being linked with a second metallic structure to cover the subsequent combustion process. In both studies, hydrogen flame temperatures are the lowest recorded. In the first test, it is because of its direct exposure to the environment, and the fluctuating behavior is caused by the change in the position of the thermocouple. However, the metallic construction of experiment 2 provides some stability for recording measurements in stage 2 but results in increased heat loss, resulting in lower H_2 flame temperatures.

The impact of reduced NH_3 adiabatic flame temperature is also reflected in the amount of hydrogen generated, as illustrated in Figure 5.5. The amount of H_2 produced in experiment 1 is more than that produced in experiment 2, reaching 0.0224 for an equivalence ratio of 1.1.

Since experiment 1 achieves higher temperatures, allows for better ammonia breakdown, which occurs at roughly 400 °C at 1 atm. It is also noticed that H_2 generation rises with the equivalence ratio due to the lack of oxygen to react with NH_3, boosting the breakdown reaction. It is worth mentioning, that the H_2 flame was also noticed in stage 2 of the experiments during the operating configuration in lean combustion. Because of the equilibrium reaction and high temperatures in the first stage, a little quantity of NH_3 might decomposes into H_2 parallel to the combustion process. The generation of hydrogen in lean combustion is also mirrored in the simulations, where Figure 5.12 demonstrates the formation of hydrogen in lean combustion even if it is promptly consumed and lower than in the rich process.

The turbulent speed of the premixed unburned gases is much greater than the turbulent flame speed in both tests and for both components NH_3 and H_2, which is required to keep the flame from blowing off. In the instance of NH_3, the swirler is used to produce turbulence in the unburned mixture, which generates recirculation zones around the flame and hence eddies, resulting in energy loss for the flame speed and flame stabilization. Figure 5.6 and Figure 5.7 illustrate that greater temperatures resulted in higher velocities for the unburned mixture (12,8 m/s the maximum unburned velocity of NH_3, at 400 K for the experiment 1 and 5,79 m/s for experiment 2). The simulated laminar flame speeds of NH_3 are modest, in contrast to its turbulent velocities but high in comparison to the literature. Simulations were done at 400 K and 1atm, with Konnov laminar flame speed being bigger (16.4 cm/s) than the Gri-Mech 3.0 (10.93 cm/s). The diffusion flame of turbulent H_2 velocities are even larger, reaching up to 25 m/s when compared to premixed NH_3-air flames, since the temperature of the unburned H_2 is approximately 600 K, whereas the temperature of the unburned NH_3-air mixture may be around 300-400 K. Similarly, the laminar velocity of the H_2 flame is lower in contrast to the literature because it does not consist of pureH_2, but it is greater than the NH_3 laminar velocity because it the H_2 properties. The velocities in experiment 2 exhibit more consistent behavior than the velocities in experiment 1, which is attributed to the lack of N_2 vent gas.

In the simulated circumstances, NH_3-air premix combustion happens at chemical times ranging from 11 to 20.4 ms. Because the major action happens in the flame at the chemical times, the residential time of the gases in the combustor is acceptable. The sensitivity study revealed that the Gri 3.0 mechanism omits important reactions to have into account in the combustion, as shown in the Konnov mechanism since they will affect the flame propagation. Nevertheless, both mechanisms show that the flame speed is substantially reliant on the $H + O_2 \leftrightarrow O + OH$ reaction, implying that the number of H, O, and OH radicals in the flame is important. The process was carried out at atmospheric pressures even though pressure decreases the O/H radical pool and the consumption of NH_3 remains the same. The presence of NH_3in the exhaust gas was below 0 to 1 ppm.

In terms of safety, NH_3 is less flammable than other fuels such as hydrocarbons or hydrogen and requires a larger concentration to exceed the explosion restrictions. Because it is exceedingly toxic, the sealing of the material and joints must ensure that no leaks occur.

Finally, as indicated in the simulations, NO_x emissions were lowered for richer mixtures. Experiment 2 had lesser emissions than experiment 1, which has up to 130000 ppm due to the absence of N_2 vent gas. However, the estimated NO_x emissions were lower than the simulated emissions but greater than the NO_x emissions observed in the experiment using the TESTO equipment. The experimental NO_x emissions were low enough without using catalysis, with the NO emission being the highest at around 700 ppm and the NO_2 maximum emissions at 16 ppm.

6 Conclusion

This research investigated the combustion of NH_3 in a pilot two-stage swirler combustor unit in response to the demand to decarbonize the marine sector with alternative fuels like NH_3 and H_2. Two tests were carried out to analyze the combustion process, and simulations were conducted using the Gri-Mech 3.0 and Konnov mechanisms to investigate the burning velocities and stability of the NH_3 flame. The h2o2 mechanism was employed to simulate the H_2 diffusion flame.

Heat loss from the combustor was roughly 39% in experiment 1 with only metallic covering for the first stage and completely isolated with SuperMag, and 67% in the experiment 2 with the metallic framework around the two combustion steps but partially isolated.

Burning velocities of NH_3 and H_2 were greater in experiment 1, where N_2 vent gas was also intermittently supplied, with unburned velocities of 12.8 m/s for NH_3 at 400 K and 1 atm and 25 m/s for H2. It is also translated into higher temperatures for experiment 1.

Rich premixed mixtures created a substantial amount of H_2, which was combusted in the combustion second step. Because of the high toxicity of NH_3, authorities must impose stricter limits on its emissions and the composition of the exhaust gas was around 1 ppm NH_3, 700 ppm NO, and 16 ppm NO_2 with the absence of a catalyst.

References

[1] ‘Pilot project: an ammonia tanker fueled by its own cargo – Ammonia Energy Association’. https://www.ammoniaenergy.org/articles/pilot-project-an-ammonia-tanker-fueled-by-its-own-cargo/ (accessed Jan. 25, 2023).

[2] M. Aarnio, ‘Environmental Aspects’, in *Cruise Ship Handbook*, M. Aarnio, Ed., in Springer Series on Naval Architecture, Marine Engineering, Shipbuilding and Shipping. Cham: Springer International Publishing, 2023, pp. 81–103. doi: 10.1007/978-3-031-11629-2_6.

[3] Sverre Alvik, Onur Özgün, Mark Irvine, and Christian Parker, ‘Hydrogen forecast to 2050. Energy Transition Outlook 2022’, DNV, Norway, 2022.

[4] K. E. Lamb, M. D. Dolan, and D. F. Kennedy, ‘Ammonia for hydrogen storage; A review of catalytic ammonia decomposition and hydrogen separation and purification’, *International Journal of Hydrogen Energy*, vol. 44, no. 7, pp. 3580–3593, Feb. 2019, doi: 10.1016/j.ijhydene.2018.12.024.

[5] W. S. Chai, Y. Bao, P. Jin, G. Tang, and L. Zhou, ‘A review on ammonia, ammonia-hydrogen and ammonia-methane fuels’, *Renewable and Sustainable Energy Reviews*, vol. 147, p. 111254, Sep. 2021, doi: 10.1016/j.rser.2021.111254.

[6] Laursen R., Barcarolo D., Paterl H., and (American Bureau of Shipping, CE Delft, and Arcsilea), ‘Potential of Ammonia as a Fuel in Shipping’. European Maritime Safety Agency, Sep. 16, 2022. Accessed: Jan. 30, 2023. [Online]. Available: www.emsa.europa.eu

[7] Sara Budinis, Alexandre Gouy, Peter Levi, Hana Mandová, and Tiffany Vass, ‘Ammonia Technology Roadmap. Towards more sustainable nitrogen fertiliser production’, International Enegy Agency, France, Oct. 2021. [Online]. Available: https://www.iea.org/reports/ammonia-technology-roadmap

[8] P. Glarborg, J. A. Miller, B. Ruscic, and S. J. Klippenstein, ‘Modeling nitrogen chemistry in combustion’, *Progress in Energy and Combustion Science*, vol. 67, pp. 31–68, Jul. 2018, doi: 10.1016/j.pecs.2018.01.002.

[9] A. Valera-Medina, H. Xiao, M. Owen-Jones, W. I. F. David, and P. J. Bowen, ‘Ammonia for power’, *Progress in Energy and Combustion Science*, vol. 69, pp. 63–102, Nov. 2018, doi: 10.1016/j.pecs.2018.07.001.

[10] A. Valera-Medina, D. G. Pugh, P. Marsh, G. Bulat, and P. Bowen, ‘Preliminary study on lean premixed combustion of ammonia-hydrogen for swirling gas turbine combustors’, *International Journal of Hydrogen Energy*, vol. 42, no. 38, pp. 24495–24503, Sep. 2017, doi: 10.1016/j.ijhydene.2017.08.028.

[11] DNV·GL and Sjøfartsdirektoratet. Norwegian Maritime Authority, ‘Ammonia as a marine fuel. Safety Handbook’, Green Shipping Programme, Norway, Revision 01, Mar. 2021. [Online]. Available: https://greenshippingprogramme.com/reports/

[12] D. Erdemir and I. Dincer, ‘A perspective on the use of ammonia as a clean fuel: Challenges and solutions’, *International Journal of Energy Research*, vol. 45, no. 4, pp. 4827–4834, 2021, doi: 10.1002/er.6232.

[13] H. Kobayashi, A. Hayakawa, K. D. K. A. Somarathne, and E. C. Okafor, 'Science and technology of ammonia combustion', *Proceedings of the Combustion Institute*, vol. 37, no. 1, pp. 109–133, Jan. 2019, doi: 10.1016/j.proci.2018.09.029.

[14] Alexei Kotchourko and Thomas Jordan, 'Hydrogen fundamentals', in *Hydrogen Safety For Energy Applications: engineering design, risk assessment, and codes and standards*, 1st ed.Amsterdam: Elsevier, 2022, pp. 19–21. Accessed: Apr. 03, 2023. [Online]. Available: https://www.sciencedirect.com/book/9780128204924/hydrogen-safety-for-energy-applications#book-description

[15] L. Kang, W. Pan, J. Zhang, W. Wang, and C. Tang, 'A review on ammonia blends combustion for industrial applications', *Fuel*, vol. 332, p. 126150, Jan. 2023, doi: 10.1016/j.fuel.2022.126150.

[16] N. Morlanés *et al.*, 'A technological roadmap to the ammonia energy economy: Current state and missing technologies', *Chemical Engineering Journal*, vol. 408, p. 127310, Mar. 2021, doi: 10.1016/j.cej.2020.127310.

[17] M. Vohra, 'Treatment of Gaseous Ammonia Emissions Using Date Palm Pits Based Granular Activated Carbon', *Int J Environ Res Public Health*, vol. 17, no. 5, p. 1519, Mar. 2020, doi: 10.3390/ijerph17051519.

[18] 'Chapter 10. Equipment Selection, Specification and Design.', in *Chemical Engineering Design: SI edition*, 5th ed.Oxford, United Kingdom: Elsevier Science & Technology, 2009, pp. 553–567. Accessed: Apr. 04, 2023. [Online]. Available: http://ebookcentral.proquest.com/lib/ucsn-ebooks/detail.action?docID=802531

[19] Tien Anh Tran, 'Research of the Scrubber Systems to Clean Marine Diesel Engine Exhaust Gases on Ships', *Research Article Journal of Marine Science: Research & Development*, vol. 7, no. Issue 6, doi: 10.4172/2155-9910.1000243.

[20] 'Scrubbing Ammonia'. https://www.crcleanair.com/pollutants/ammoniaamines/ (accessed Apr. 04, 2023).

[21] C. Wang, Y. Ju, and Y. Fu, 'Comparative life cycle cost analysis of low pressure fuel gas supply systems for LNG fueled ships', *Energy*, vol. 218, p. 119541, Mar. 2021, doi: 10.1016/j.energy.2020.119541.

[22] 'Unidad de combustión de gas'. https://www.alfalaval.es/productos-y-soluciones/transferencia-de-calor/quemadores/unidad-de-combustion-de-gas/ (accessed Apr. 06, 2023).

[23] 'Gas Combustion Unit | Sicherer Transport von Erdgas auf See | SAACKE- SAACKE Group'. https://www.saacke.com/de/marine-systems/produktuebersicht-marine/gas-combustion-unit-gcu (accessed Apr. 06, 2023).

[24] Damien Feger, 'Gas Combustion Units: High Performance Technologies For Safe Disposal Of Excess Boil Off Gas On The New Generation Of LNG Carriers.', Snecma, Vernon, France. Accessed: Apr. 06, 2023. [Online]. Available: http://www.ivt.ntnu.no/ept/fag/tep4215/innhold/LNG%20Conferences/2007/fscommand/PO_09_Feger_s.pdf

[25] S. McAllister, J.-Y. Chen, and A. C. Fernandez-Pello, *Fundamentals of Combustion Processes*. in Mechanical Engineering Series. New York, NY: Springer New York, 2011. doi: 10.1007/978-1-4419-7943-8.

[26] C. Zamfirescu and I. Dincer, ‘Using ammonia as a sustainable fuel’, *Journal of Power Sources*, vol. 185, no. 1, pp. 459–465, Oct. 2008, doi: 10.1016/j.jpowsour.2008.02.097.

[27] P. Glarborg, ‘The NH3/NO2/O2 system: Constraining key steps in ammonia ignition and N2O formation’, *Combustion and Flame*, p. 112311, Aug. 2022, doi: 10.1016/j.combustflame.2022.112311.

[28] I. Lucentini, X. Garcia, X. Vendrell, and J. Llorca, ‘Review of the Decomposition of Ammonia to Generate Hydrogen’, *Ind. Eng. Chem. Res.*, vol. 60, no. 51, pp. 18560–18611, Dec. 2021, doi: 10.1021/acs.iecr.1c00843.

[29] T. E. Bell and L. Torrente-Murciano, ‘H2 Production via Ammonia Decomposition Using Non-Noble Metal Catalysts: A Review’, *Top Catal*, vol. 59, no. 15, pp. 1438–1457, Sep. 2016, doi: 10.1007/s11244-016-0653-4.

[30] ‘Hydrogen-oxygen reaction mechanism and its implication to hydrogen engine combustion’, *International Journal of Hydrogen Energy*, vol. 21, no. 8, pp. 703–715, Aug. 1996, doi: 10.1016/0360-3199(95)00138-7.

[31] Frank P. Incropera, David P. Dewitt, Theodore L. Bergman, and Adrienne S. Lavine, *Incropera’s Principles of Heat and Mass Transfer*, Global Edition. Singapore: Wiley, 2017.

[32] T. Poinsot and D. Veynante, *Theoretical and Numerical Combustion*, 2nd ed. Philadelphia: R.T. Edwards, Inc., 2005.

[33] Alexei Kotchourko and Thomas Jordan, *Hydrogen Safety For Energy Applications. Engineering design, risk assessment, and codes and standards*, 1st ed. Amsterdam: Elsevier, 2022.

[34] X. Han, Z. Wang, Y. He, Y. Liu, Y. Zhu, and A. Konnov, ‘The temperature dependence of the laminar burning velocity and superadiabatic flame temperature phenomenon for NH3/air flames’, *Combustion and Flame*, vol. 217, pp. 314–320, Jul. 2020, doi: 10.1016/j.combustflame.2020.04.013.

[35] Odd Ivar Lindløv and Nina C Leander, ‘NH3 Cracker Phase 1 Report’, Wärtsilä Moss AS, Moss, Research and Development Version 2, Dec. 2021.

[36] Odd Ivar Lindløv, ‘Ammonia Release Mitigation System’, Wärtsilä Moss, Dec. 19, 2022.

[37] Odd Ivar Lindløv, ‘Ammonia gas combustion unit-Testing phase 2 [Draft]’, Wärtsila Moss, Moss, Jan. 2023.

[38] P. Kumar and T. R. Meyer, ‘Experimental and modeling study of chemical-kinetics mechanisms for H2–NH3–air mixtures in laminar premixed jet flames’, *Fuel*, vol. 108, pp. 166–176, Jun. 2013, doi: 10.1016/j.fuel.2012.06.103.

[39] C. Duynslaegher, H. Jeanmart, and J. Vandooren, ‘Flame structure studies of premixed ammonia/hydrogen/oxygen/argon flames: Experimental and numerical investigation’, *Proceedings of the Combustion Institute*, vol. 32, no. 1, pp. 1277–1284, Jan. 2009, doi: 10.1016/j.proci.2008.06.036.

[40] N. O. of D. and Informatics, ‘Bienvenido al Libro del Web de Química del NIST’. https://webbook.nist.gov/ (accessed May 14, 2023).

Appendices

Appendix A: Task description

FM606 Master's Thesis

Title: Ammonia vent handling for carbon-free shipping

USN supervisor: Assoc. Prof. Joachim Lundberg

External partner: Wärtsilä Moss AS

Task background:
Ammonia is considered one of the carbon-free fuels that will take a significant share of the global marine fuel consumption. However, due to its toxicity, Ammonia has additional requirements not seen for regular hydrocarbon fuels. Also, hydrogen can be a intermediate in ammonia fueld vessels.
The essential difference, e.g., LNG, is the 30ppm allowable upper limit of fuel (ammonia) released to ambient air through vent and vent systems from operational releases. LNG does not need similar stringent emission regulations.
Operational releases are defined as releases from fuel bunker system during purging operations (gassing up and gas freeing), handling of minor liquid releases from Thermal Relief Valves, and handling of ammonia vapor in the event of an ESD, including purge from engines.
A Gas Combustion Unit is expected to compete with, e.g., an ammonia scrubber solution. Still, for bunker and other IGC vessels and deep sea shipping, a GCU is likely to be the preferred technology and probably also for some IGF segments due to a more compact design than its alternative.

The ammonia Gas Combustion Unit (GCU), or thermal oxidizer, is a device that will decompose ammonia vent gas back into nitrogen and hydrogen, where the hydrogen is oxidized in a final stage. Emissions will then be water, nitrogen, and small amounts of ammonia slip and NOx from combustion. The pilot flame, providing heat for the process, will be fueled by ammonia, eliminating any soot, CO, or CO2 emissions.

Current technology is still developing, and Wärtsilä wants to cooperate with USN students to optimize the reactor's design based on advanced theoretical calculations.

Task description:

- Literature study on ammonia combustion reviewing previous works and relevant combustion theory.
- Simulate the reaction kinetics using Cantera to investigate the reaction pathways.
- Perform measurements on the small pilot facility in Moss in cooperation with Wärtsilä
- Determine important parameters for improving the reactor design, such as residential time, material, pressure, temperature.

Student category: EET or PT students

The task is suitable for students not present at the campus (e.g., online students): No

Practical arrangements:

Might need a car for transport

Supervision:

As a general rule, the student is entitled to 15-20 hours of supervision. This includes necessary time for the supervisor to prepare for supervision meetings (reading material to be discussed, etc).

Appendix B: Specific heat capacity parameters

$$C_p^0 = A + BT + CT^2 + DT^3 + E/T^2$$

C_p =Heat capacity [J/mol·K]

T =Temperature [K]/1000

Table B: Heat capacity parameters. [40]

Component	Temperature interval [K]	A	B	C	D	E
NH3	**298-1400**	19.99563	49.77119	-15.37599	1.921168	0.189174
	1400-6000	52.02427	18.48801	-3.765128	0.248541	-12.45799
O2	**100-700**	31.32234	-20.23531	57.86644	-36.50624	-0.007374
	700-2000	30.03235	8.772972	-3.988133	0.788313	-0.741599
H2O	**298-500**	-203.606	1523.29	-3196.413	2474.455	3.855326
	500-1700	30.092	6.832514	6.793435	-2.53448	0.082139
	1700-600	41.96426	8.622053	-1.499978	0.098119	-11.15764
H2	**298-1000**	33.066178	-11.36342	11.432816	-2.772874	-0.158558
	1000-2500	18.563083	12.257357	-2.859786	0.268238	1.97799
NO	**298-1200**	23.83491	12.58878	-1.139011	-1.497459	0.214194
	1200-6000	35.99169	0.95717	-0.148032	0.009974	-3.004088
NO2	**298-1200**	16.108557	75.89525	-54.3874	14.30777	0.239423
	1200-6000	56.82541	0.738053	-0.144721	0.009777	-5.429911
N2O	**298-1400**	27.67988	51.14898	-30.34454	6.847911	-0.157906
	1400-6000	60.30274	1.034566	-0.192997	0.01254	-6.860254
N2	**100-500**	28.98641	1.853978	-9.647459	16.63537	0.000117
	500-2000	19.50583	19.88705	-8.598535	1.369784	0.527601

Appendix C: Experimental structure and dimensions of experiment 2.

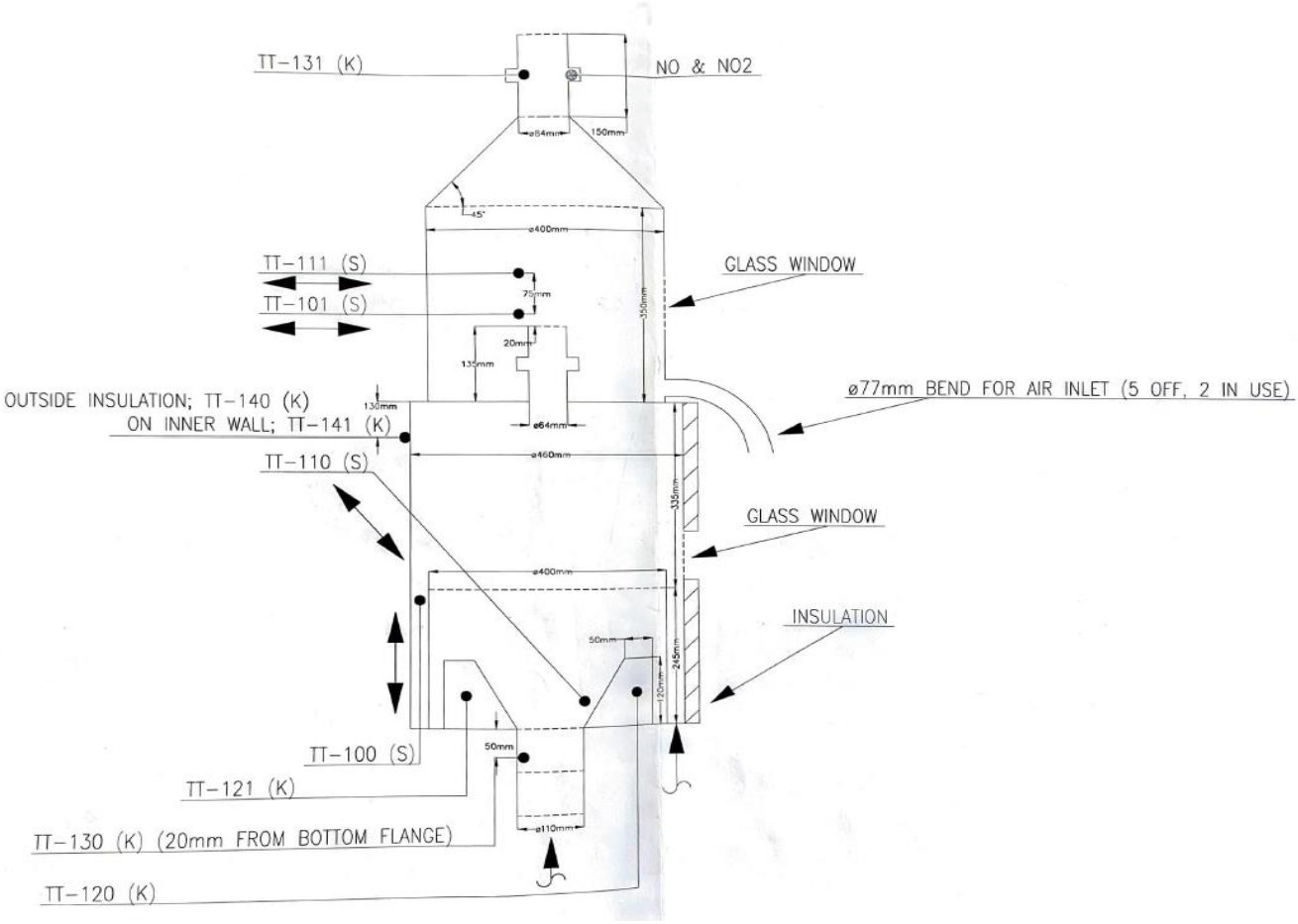

Figure 1: Dimensions and thermocouple locations for the experimental configuration 2.